Dalton Transactions

ROYAL SOCIETY OF CHEMISTRY

PERSPECTIVE

View Article Online
View Journal | View Issue

Cite this: *Dalton Trans.*, 2025, **54**, 458

Bicyclic (alkyl)(amino)carbenes (BICAACs): synthesis, characteristics, and applications

Ankita Sharma,[a] Unnikrishnan Nair K[a,b] and Subrata Kundu *[a]

Carbenes in general and isolable NHCs (N-heterocyclic carbenes) in particular have been useful ligands in recent years. The emergence of CAACs [cyclic(alkyl)(amino)carbenes], BICAACs [bicyclic(alkyl)(amino)carbenes], and many other carbenes has marked revolutionary milestones in this field. These carbenes possess an intriguing blend of highly electrophilic and nucleophilic characteristics, owing to their remarkably narrow HOMO–LUMO energy gap. The isolation and characterization of these carbenes hold significance not only due to their fascinating electronic properties but have demonstrated their prowess across various domains, including isolation of transition metal complexes, medicinal applications, catalysis, and radical stabilization. While the chemistry of 5-membered NHCs and CAACs has been extensively explored, the investigation of BICAACs has just begun. This review covers the synthesis, characterization, and reactivity of BICAACs and outlines the diverse applications of BICAACs in organometallic chemistry, metal-free catalysis, and main-group chemistry.

Received 23rd September 2024,
Accepted 7th November 2024

DOI: 10.1039/d4dt02696a

rsc.li/dalton

1. Introduction

Carbenes were thought to be laboratory curiosities until the first isolable carbene, {bis(diisopropylamino)phosphino}(trimethylsilyl) carbene, was prepared by Bertrand *et al.* in 1988.[1] This remarkable compound was successfully isolated in liquid form and stabilized through favourable interactions with adjacent heteroatoms [P and Si], resulting from double-bond formation.[1] In 1991, Arduengo *et al.* reported an isolable singlet carbene, which was characterized by the single crystal XRD technique for the first time.[2] This pivotal achievement has paved the way for the isolation of many other types of singlet carbenes.[3] Among the isolated carbenes, the so-called N-heterocyclic carbenes (NHCs) have found applications in medicine and materials science.[4–6] In 2005, Bertrand *et al.* reported a new family of stable five-membered carbenes [cyclic(alkyl)(amino)carbenes (CAAC)], which result from the replacement of one of the two amino substituents of classical N-heterocyclic carbenes (NHCs) by a quaternary carbon atom.[7] CAACs exhibit superior electrophilic and nucleophilic characteristics compared to NHCs.[8]

[a]*Department of Chemistry, Indian Institute of Technology Delhi, Hauz Khas, New Delhi 110 016, India. E-mail: subrata@iitd.ac.in*
[b]*Department of Chemistry, Ashoka University, Sonepat, Haryana-131029, India*

Ankita Sharma

Ankita Sharma was born in Noida, Uttar Pradesh, India. She did her graduation in Chemistry (Hons) in 2018 from Miranda House, University of Delhi, and Master's from the Indian Institute of Technology Delhi in 2021. Currently she is pursuing her Ph.D. under the supervision of Dr Subrata Kundu at the Indian Institute of Technology Delhi.

Unnikrishnan Nair K

Unnikrishnan Nair K completed his M.Sc. in Analytical Chemistry from the University of Kerala in 2021. In December 2022, he joined Dr Subrata Kundu's research group at the Indian Institute of Technology Delhi as a project assistant. Presently, he serves as a project associate in the research group of Dr Munmun Ghosh at Ashoka University, Haryana.

Later, in 2017, Bertrand's group introduced bicyclic(alkyl)(amino)carbenes (BICAACs) with a bicyclo[2.2.2]octane framework.[9] Furthermore, BICAACs have superior σ-donating and π-accepting characteristics in comparison with CAACs and consequently NHCs. Quantum chemical calculations reveal that among the carbene ligands whose chemistry has been explored to a decent extent, BICAACs have high energy HOMOs (higher nucleophilicity and more σ-donating) and low energy LUMOs (higher electrophilicity and more π-accepting). The singlet–triplet energy gaps ($\Delta E_{S/T}$) in BICAACs are smaller than those in NHCs and slightly smaller than those in 5-membered CAACs (Fig. 1).[9]

Today, carbenes are among the most powerful tools in chemistry, used in materials science, catalysis, and the isolation of compounds in their lower oxidation states.[19–23] Furthermore, in numerous instances, it has been observed that CAACs and BICAACs are very effective in stabilizing paramagnetic species, activating small molecules, and forming enthalpically strong bonds due to their superior electronic and steric characteristics.[19] Comparative studies of the reactivity of several stable carbenes have been conducted in recent years, and it has been found that, frequently, CAACs and BICAACs exhibit different reactivity from NHCs. Furthermore, CAAC and BICAAC coordinated catalysts frequently outperformed their NHC-coordinated catalyst counterparts.[19a–k]

The chemistry of NHCs and five-membered CAACs is extensively covered in numerous reviews and books; therefore, we have not included CAAC-related works in this review.[3,24–31] Since the chemistry of BICAACs is relatively new and lacks a dedicated review despite its reported applicability on various occasions, we focus on reports related to BICAACs. Additionally, the relevant properties of IPr (1,3-bis(2,6-diisopropylphenyl)imidazol-2-ylidene), CAACs and 6-CAACs (6-CAAC = six-membered cyclic(alkyl)(amino)carbene) have been included on a few occasions for comparative purposes. The content of this review has been divided into the following sections: (1) Introduction, (2) Synthesis of BICAACs, (3) Evaluation of the electronic properties of BICAACs, (4) BICAAC metal complexes, (4) BICAACs as metal-free catalysts, (5) BICAAC-supported main-group compounds, and (6) Conclusions.

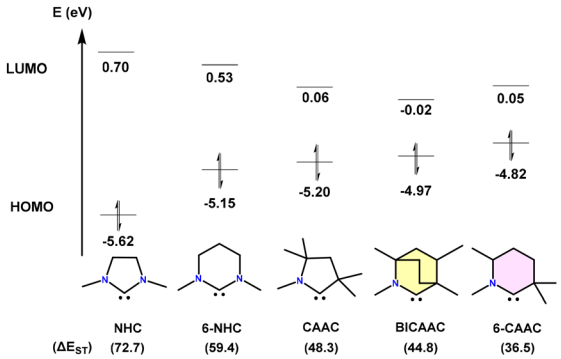

Fig. 1 HOMO–LUMO gap (eV) and $\Delta E_{S/T}$ (kcal mol^{-1}) of NHC, 6-NHC, CAAC, BICAAC, and 6-CAAC (calculated at the B3LYP/def2-TZVPP level of theory).

Various notations have been used in the literature to depict the bond between BICAACs and a central atom. In this review, we have chosen to use an arrow for consistency. However, in cases where significant π-back donation occurs, we followed the literature and used a double bond.

2. Synthesis of BICAACs

In 2017, Bertrand and co-workers reported the synthesis of BICAACs, which is presented in Scheme 1.[9] The reaction of trivertal and 2,6-diisopropylaniline under acidic conditions formed an imine overnight. This imine, when treated with ^{n}BuLi at −78 °C and then alkylated with methyl chloride, produced an alkylated trivertal imine. Cyclization of the alkylated trivertal imine under anhydrous acidic conditions, followed by anion exchange with sodium tetrafluoroborate, provided the

Subrata Kundu

Subrata Kundu was born in Bankura, West Bengal, India. He received his Ph.D. degree in 2015 from the Indian Institute of Technology Kanpur under the guidance of Prof. V. Chandrasekhar and Prof. Sandeep Verma. After a couple of post-doctoral positions in the research groups of Prof. H. W. Roesky and Prof. Ian Manners, in December 2019, Subrata joined IIT Delhi as an assistant professor. Presently, he is working in the area of low-valent main-group chemistry.

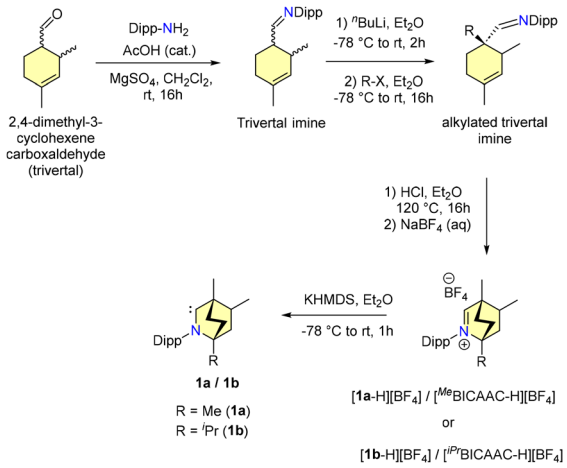

Scheme 1 Synthesis of a BICAAC.

iminium salts [**1a**-H][BF_4] and [**1b**-H][BF_4]. Deprotonation of [**1a**-H][BF_4] using KHMDS generated a free BICAAC (**1a**). The free carbene **1a** was found to be stable in the solid state when stored under an inert atmosphere. Moreover, it was structurally characterized using single crystal X-ray diffraction. The yield of BICAACs for multi-gram synthesis from the primary starting materials varies from 15 to 33%. The $^{13}C\{^1H\}$ NMR spectrum of **1a** showed a singlet at 334 ppm, which is deshielded compared to CAAC (320 ppm).[7]

3. Evaluation of the electronic properties of BICAACs

As discussed in the Introduction, the BICAAC's highest occupied molecular orbital (HOMO) and lowest unoccupied molecular orbital (LUMO) have higher and lower energies, respectively, than CAACs and imidazole-based carbenes. This is also demonstrated by a considerable decrease in the singlet–triplet gap from 49.2 kcal mol^{-1} for CAACs to 45.7 kcal mol^{-1} for BICAACs for the DFT optimized model compounds as discussed in Fig. 1.[26] BICAACs have higher σ-donation and π-acceptance than CAACs, possibly due to their broader carbene bond angle (106.9° for CAAC *vs.* 110.2° for BICAAC). The 6-CAAC has a 117.9° carbene bond angle.[10] It should be noted that increasing the carbene bond angle of NHCs leads to higher p-character in both the HOMO and LUMO, resulting in a smaller ΔE_{ST}.[32]

Tolman electronic parameters (TEPs) provide valuable information for comparing the electron-donating abilities of carbenes. TEPs were developed for the evaluation of the electron-donating ability of phosphines in phosphine coordinated metal-carbonyl complexes (by measuring the infrared stretching frequencies of carbonyl ligands) and were also used to determine the overall electron-donating ability of carbene ligands. Accordingly, TEPs were obtained from various square planar complexes, [(carbene)$Rh(CO)_2Cl$]. It was found that the overall electron donation ability of ^{Ad}6-CAAC is better than that of ^{Me}BICAAC. However, ^{Me}BICAAC demonstrates superior donor ability to ^{iPr}NHC, ^{cy}CAAC, and acyclic diaminocarbene (^{iPr}ADCs) (Fig. 2).[8–14]

Later, Jazzar and Bertrand *et al.* reported an excellent strategy to determine the basicity of carbenes by a proton exchange reaction between a free carbene and a carbene conjugate acid.[15] In this reaction, the equilibrium will move in the direction of the more basic carbene, forming the corresponding conjugate acid, which could be monitored by $^{13}C\{^1H\}$ NMR.

Carbenes were found to be best placed in the sequence 6-CAAC > BICAAC > CAAC > NHC in strong connection with their theoretically expected basicity after completing a few strategic reactions (Scheme 2).

Comparing the $^{31}P\{^1H\}$ NMR signals of carbene–phenylphosphinidene adducts and the $^{77}Se\{^1H\}$ NMR chemical shift of carbene–selenium adducts has proved to be an effective method for determining a carbene's π-accepting characteristics.[16,17] The second technique is beneficial since

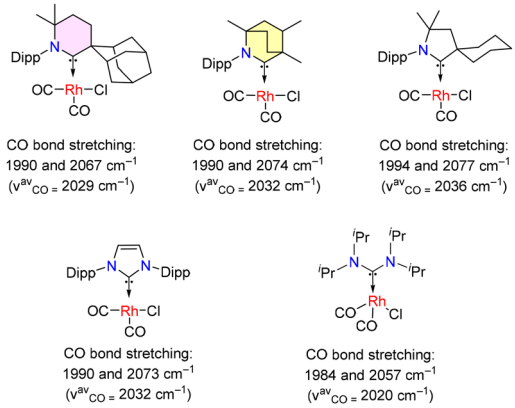

Fig. 2 C–O stretching frequencies of carbene coordinated $Rh(CO)_2Cl$ complexes.

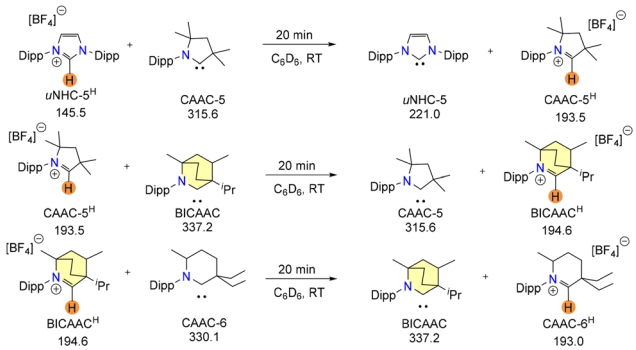

Scheme 2 Proton exchange reactions between a carbene and carbene conjugate acid. $^{13}C\{^1H\}$ chemical shifts of the carbenic carbon in ppm units have been mentioned.

the $^{77}Se\{^1H\}$ NMR scale is wider (Δ > 850 ppm), and the carbene selenium adduct is simple to generate. However, it should be kept in mind that ^{77}Se is poisonous, and $^{77}Se\{^1H\}$ NMR is not as readily accessible as ^{31}P NMR.[17] Additionally, the presence of non-classical hydrogen bonds (NCHB) in carbene–selenium adducts results in noticeable downfield shifts in $^{77}Se\{^1H\}$ NMR spectra, which disturbs the Se scale and makes it challenging to examine the π-accepting characteristics of the carbene family. Furthermore, it is important to note that the choice of NMR solvent for recording the $^{77}Se\{^1H\}$ NMR spectrum is highly significant. A substantial change in the chemical shift (30 ppm) was found for the compound $(^iPr_2N)_2C{=}Se$ when comparing $CDCl_3$ with acetone-d6.[33] In order to determine the π-acidity of carbene ligands, it is thus far more realistic to use the ^{31}P chemical shifts of the carbene–phosphinidene adducts. It is evident that an increase in the carbene's π-accepting ability favors the back donation of the phosphorus atom's lone pair to the vacant p-orbital of the carbene center. As a result, the ^{31}P NMR chemical shift of carbene–phosphinidene adducts should offer a simple approach for assessing the carbene's π-accepting properties: the more π-accepting the carbene is, the further downfield the

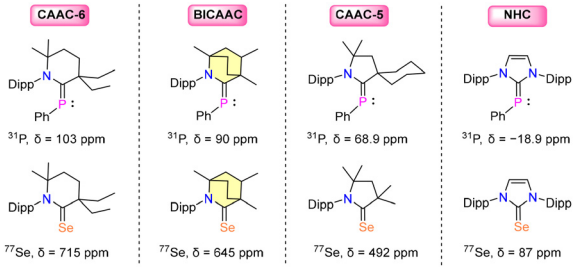

Fig. 3 $^{31}P\{^1H\}$ and $^{77}Se\{^1H\}$ NMR chemical shifts of carbene·(PPh) and carbene·(Se) adducts.

phosphorus nucleus's chemical shift will be. The $^{31}P\{^1H\}$ and $^{77}Se\{^1H\}$ chemical shifts indicate the following order [6-CAAC > BICAAC > CAAC > NHC] of the π-accepting properties of the carbene ligands (Fig. 3).[8–11]

Mondal and coworkers developed a methodology to establish the σ-donating and π-accepting properties of 5-membered CAACs using ^{15}N NMR.[18] This method describes that if a carbene exclusively functions as a σ-donor with species E, the formally unoccupied $2p^{\pi}(C)$ orbital is mainly stabilized by nitrogen π-donation. This results in nitrogen being electron deficient and a low-field ^{15}N NMR signal. Conversely, when the carbene interacts with σ accepting and π-donating substances, the latter will also donate electrons to the empty $2p^{\pi}(C)$ orbital. This will result in a weaker π-donation by the nitrogen and a higher field ^{15}N signal.[18] Unfortunately, this method of exploring the electronic properties of BICAACs has yet to be explored.

4. BICAAC metal complexes

Coinage metal–carbene complexes have applications in medicinal chemistry due to their cytotoxic properties[34a–c] and are interesting candidates for application in OLEDs due to their unique photophysical properties.[34d,e] Several carbene–Au/Cu complexes are explored as metal catalysts.[35–37] Along with the synthesis of BICAACs (Scheme 1), Bertrand *et al.* also reported the synthesis of BICAAC complexes of coinage metals in the same paper.[9]

A homoleptic, bis-carbene complex $[(^{Me}BICAAC)_2Cu][CuBr_2]$ {**2**[$CuBr_2$]} was isolated from the reaction of free carbene **1a** with $CuBr(SMe_2)$ (Scheme 3a). Complex **2**[$CuBr_2$] exists as a mixture of diastereomers. In a similar reaction, a heteroleptic covalent, mono-carbene complex (^{iPr}BICAAC)CuBr (**3**) was obtained using a bulky ^{iPr}BICAAC (**1b**). A heteroleptic gold complex (^{Me}BICAAC)AuPh (**4**) was synthesized by the reaction of the free carbene (**1a**) with $AuPh(PMe_3)$ in THF (Scheme 3). Later, in 2020, Singh *et al.* also reported similar types of BICAAC coinage-metal complexes (Scheme 3b).[38a] Heteroleptic complexes (^{Me}BICAAC)CuCl (**5**) and (^{Me}BICAAC)CuI (**6**) were formed as the major products with some minor quantities of **2**[CuI_2] in the reaction of copper halides (CuCl and CuI) and **1a** in equimolar amounts in THF (Scheme 3). It is known that Group-11 carbene metal complexes of type (carbene)MX (X = halides) slowly convert into $[(carbene)_2M]^+[MX_2]^-$.[38b] Similarly, an ionic gold complex **7**[$AuCl_2$] was formed in the reaction of equimolar amounts of $AuCl(SMe_2)$ and ^{Me}BICAAC in toluene and the formation of **7**[$AuCl_2$] proceeds through the disproportion of intermediate mono-carbene gold chloride.[38a] Homoleptic complex **2**[PF_6] can be synthesized exclusively through the reaction of a THF solution of **5**, ^{Me}BICAAC, and KPF_6 in equimolar concentrations for 10 h (Scheme 3b). It is important to note that, unlike BICAACs, no ionic complex formation was seen during the equimolecular interaction of ^{cy}CAAC and CuCl in THF, which solely produced a colorless complex [(^{cy}CAAC)CuCl].[38] Single crystal analysis of **2**[$CuBr_2$] shows a C–Cu–C bond angle of 180.0° but in **3** and **5**, the C–Cu–X bond angles are 176.6° and 176.5°, respectively. In $\mathbf{2}^+$ and $\mathbf{7}^+$, an inversion center is located at the metal in both complexes. The positioning of the sterically demanding Dipp groups within the crystal units leads to infrequent (sp^3)C–H···Cu/(sp^3)C–H···Au intermolecular or intramolecular anagostic and pre-agostic binding interactions. The $C_{carbene}$–Cu bond distance in **5** is 1.889(5) Å, which is close to the $C_{carbene}$–Cu distance of 1.888(3) found in [(^{cy}CAAC)CuCl]. The solution UV-Vis absorption spectra display bands between 312 nm and 364 nm, attributed to (σ + X)-π* charge transfer in complexes **5** and **6**, and metal to ligand charge transfer (MLCT) transitions in **2**[PF_6] and **7**[$AuCl_2$]. However, complexes **5**, **6**, **2**[PF_6] and **7**[$AuCl_2$] exhibit broad absorption bands between 250 and 640 nm in the solid state. These unexpected bands may be caused by the mixing of intra-ligand interactions with certain weak non-covalent interactions.[38]

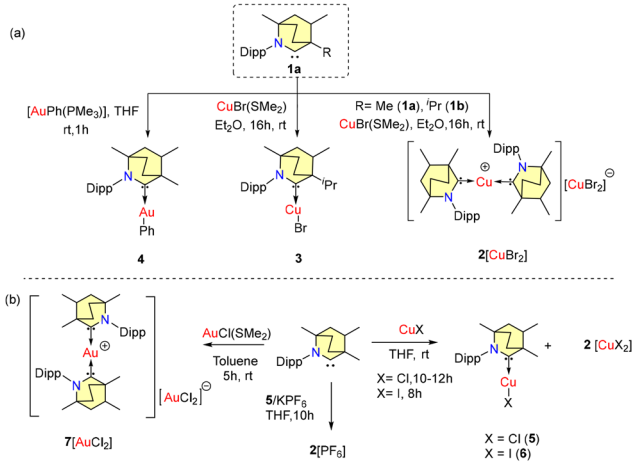

Scheme 3 Synthesis of Cu/Au-BICAAC complexes.

In 2018, Bertrand *et al.* reported that (BICAAC)$CuBH_4$ (**8a**) could catalytically convert CO_2 to formate in synergy with the Lewis pair DBU/BCF (TON-118) (Scheme 4).[39] Complex **8a** was found to exhibit higher activity compared to the reduction achieved solely with the Lewis pair DBU/BCF (TON-66) at 100 °C. The synthesis of catalyst **8a** is given in Scheme 4b. The characterisation of **8a** was done by single crystal X-ray diffraction. The ^1H NMR analysis of **8a** showed a broad quartet peak

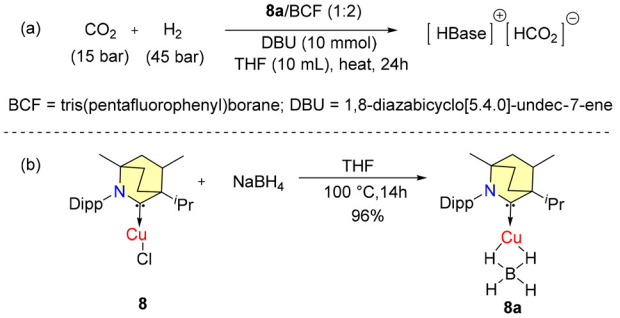

Scheme 4 Reduction of CO_2 to formic acid using **8a**.

with a chemical shift of 54 ppm for B–H hydrogens with $^1J_{B-H}$ = 81.51 Hz.

However, the efficiency of **8a** was found to be lower than that of the corresponding catalytic systems based on ^{Et2}CAAC (TON-305).[39] The reduction of carbon dioxide to formic acid using copper hydrides as catalysts was not feasible because of the low stability, catalyst deactivation, and the inability of copper to activate H_2.

In 2020, Bochmann and coworkers investigated the photophysical properties of BICAAC-coinage metal amides.[40a] Metal complexes **8–13** are synthesized according to Scheme 5a. All complexes were found to be stable in air and solvent media.

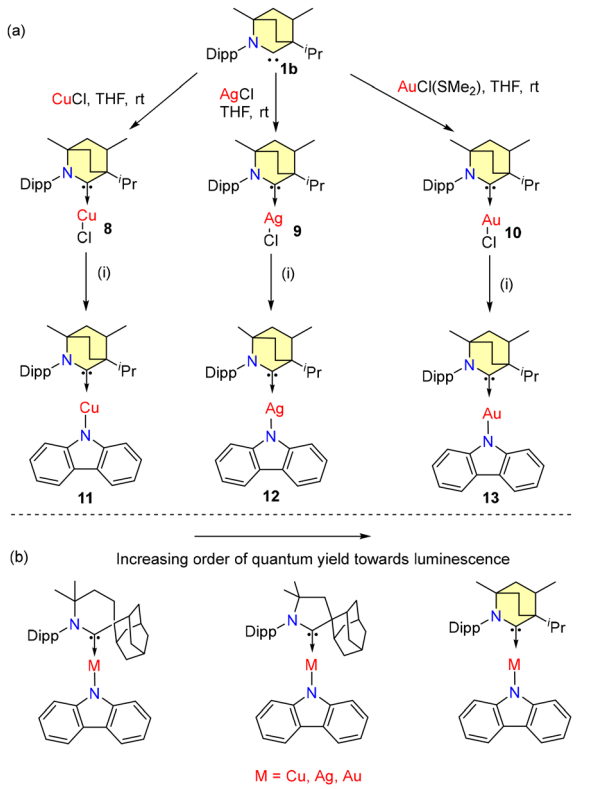

Scheme 5 (a) Synthesis of BICAAC-metal amides: (i) carbazole, ^{t}BuOK, THF, and 3 h. (b) Relative photoluminescence properties.

Notably, all the amide complexes **11–13** showed high stability upon irradiation with hard UV light at 290 nm. Among them, the gold complex **13** showed the highest stability in soft UV light. **11** showed green luminescence and 100% quantum yield (Φ_{PL}) in the solution phase. Complexes **12** and **13** showed a quantum yield of 82% and 100%, respectively (Scheme 5b).[40b]

The CAAC-6 ligated metal carbazolate complex exhibited yellow luminescence and a low Φ_{PL} (3.6% to 21.8%). In 2022, Cui *et al.* investigated the luminescence mechanism of **11** by conducting DFT/multireference configuration interaction studies, which revealed thermally activated delayed fluorescence (TADF).[41]

A highly selective protoboration of substituted terminal alkynes utilizing CAAC or BICAAC-supported copper catalysts was reported by the Bertrand group in 2021.[42] Numerous aryl substrates, such as substituted aryl alkynes, alkyl alkynes, 2-ethynylnaphthalene, and heterocycles, produced the desired Markovnikov product with superior yields (51%–94%), showcasing a remarkable degree of α-selectivity (Scheme 6). In protoboration of alkyl substituted terminal alkynes (^{Et2}CAAC)CuCl, (^{Et2}6-CAAC)CuCl and (^{CHMePh}BICAAC)CuCl (**8b**) exhibited high conversion (yield) with comparable selectivity, which is different from the result obtained with (NHC)CuCl catalysts (Scheme 7). The catalytic activities of (^{iPr}BICAAC)CuCl (**8**) and (^{CHMePh}BICAAC)CuCl (**8b**) towards protosilylation of 5-phenyl-1-pentyne showed comparable α-selectivity, while a lower yield (50%) was obtained with **8b** compared to **8** (99%) under the same reaction conditions (Scheme 7). Later in 2022, the same group reported highly α-selective methylboration of 5-phenyl-1-pentyne with **8** and **8b** (Scheme 8).[43]

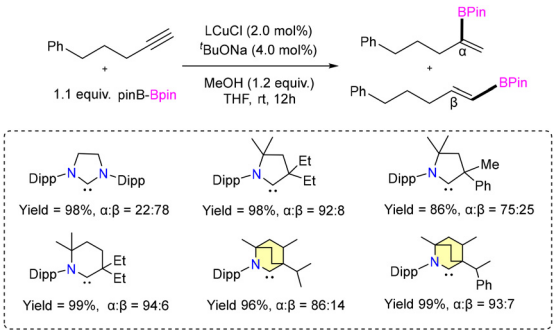

Scheme 6 Relative selectivity of protoboration using (carbene)CuCl as the catalyst.

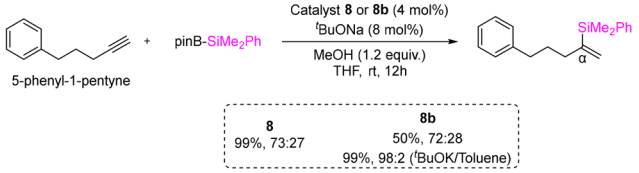

Scheme 7 Protosilylation of 5-phenyl-1-pentyne.

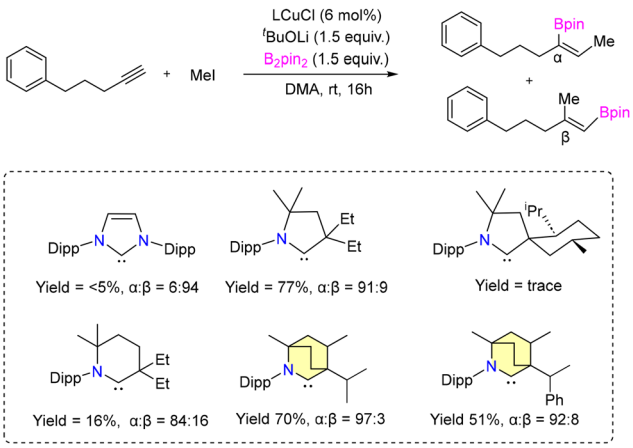

Scheme 8 α-Selective methylboration of 5-phenyl-1-pentyne.

No allylboration was observed. The study revealed that the presence of Lewis basic functional groups tends to a reduction in the catalytic efficacy of **8b**. Interestingly, ^{Et2}CAAC-copper catalysts outperformed BICAAC-based catalysts in methylboration and allylboration with a broader substrate scope, selectivity, and product yield.[43] The Bertrand group reported hydroamination and hydrohydrazination of alkynes catalyzed by BICAAC-gold catalysts in 2020.[44] Hydroamination was conducted with optimized catalyst conditions of 2.5 mol% of **10**/KBAr^F in benzene (Scheme 9). Remarkably, catalyst **10** demonstrated superior performance compared to previously known catalysts based on NHC and PPh_3 due to better steric and electronic properties. Various substrates like aryl-substituted terminal alkynes reacted efficiently with aniline derivatives at 20 °C to afford the corresponding products in a very high quantitative yield. However, with alkyl substituted terminal alkynes, higher temperature was favored for better conversions. Similarly, internal alkynes reacted slowly and demanded higher temperatures and longer reaction times. Meanwhile, the conversion of low-boiling alkynes like ethoxy alkyne was achieved even at room temperature. Notably, sterically crowded anilines (Mesityl-NH_2 and Dipp-NH_2), electron-poor perfluoro anilines (C_6F_5-NH_2) and dichloroanilines ($C_6H_3Cl_2$-NH_2) also afforded very high yields (Scheme 9a).[44] Complex **10** efficiently catalyzed the hydrohydrazination of alkynes, where 1,1-disubstituted hydrazines were found to be less reactive (Scheme 9b). In the same report, they found that carbene–π alkyne cationic gold complexes are pivotal intermediates in both hydroamination and hydrohydrazination reactions. Notably, compounds **10** and **10a** engage in the formation of cationic adducts, namely **14**[BF_4] and **14a**[BF_4], when reacting with *n*-hexyne (Scheme 10). It was noteworthy that **14**[BF_4] remained stable in air for up to four days, while **14a**[BF_4] decomposed after two days, yielding inactive bis-ligated cationic gold complex **7**[BF_4] and Au(0) nanoparticles, as depicted in Scheme 10.[44]

To confirm the existence of the active catalyst, gold cationic complexes of diphenylacetylene **15**[BAr^F] and **15**[BF_4] were synthesized (Scheme 11) and the molecular structure of **15**[BAr^F] was confirmed by single crystal X-ray diffraction studies.

The interaction between *p*-tolyl-acetylene and **10** yielded **16**[BAr^F], which then underwent subsequent reactions with *p*-toluidine and tosyl hydrazine, resulting in the anticipated products. Intriguingly, this process also led to the formation of Werner adducts, specifically **17**[BAr^F] and **18**[BAr^F], as illustrated in Scheme 12. Compounds **17**[BAr^F] and **18**[BAr^F] were structurally characterized by single-crystal X-ray diffraction.

In 2022, Singh *et al.* documented Negishi cross-coupling reactions catalyzed by BICAAC-nickel complexes.[45] By combining free carbene **1a** with the corresponding nickel halides in

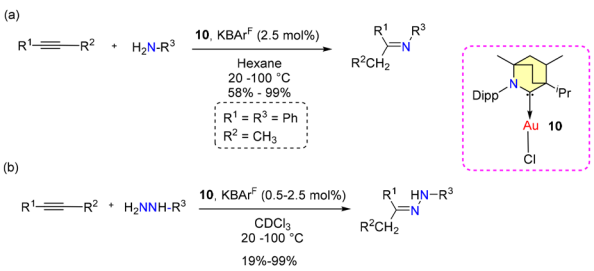

Scheme 9 (a) Hydroamination and (b) hydrohydrazination using **10**.

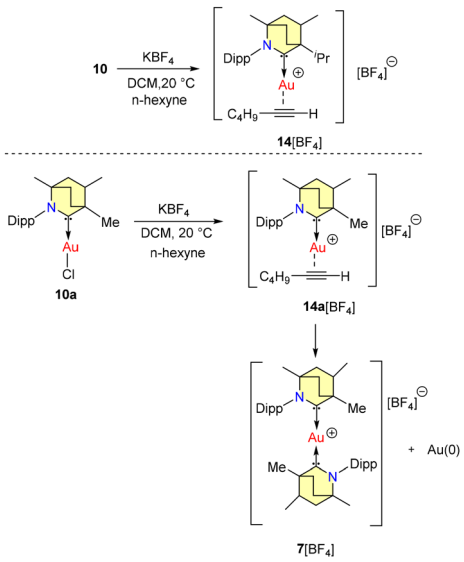

Scheme 10 Formation of cationic adducts of BICAAC supported Au(I) and ^{n}hexyne.

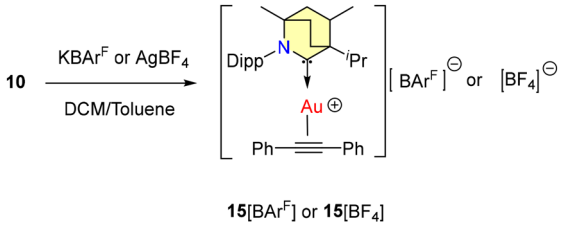

Scheme 11 Formation of cationic complexes of diphenylacetylene.

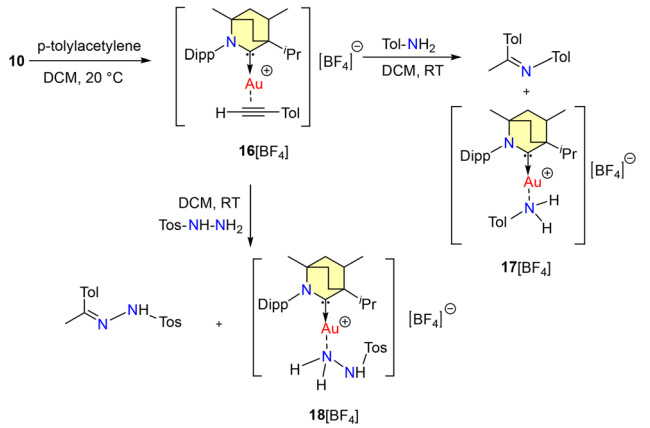

Scheme 12 Formation of Werner adducts.

THF at room temperature, a mixture of rotamers (**19–21a**) was generated (Scheme 13).

In the case of complexes **19–21**, the Dipp group was positioned in a *trans*-anti configuration, leading to a square planar geometry, while a *trans–syn* orientation was observed in **19a–21a**. Remarkably, these rotamers remained non-interconvertible within the temperature range of −60 to 60 °C. The subsequent reduction of compounds **19–21** with KC_8 led to the formation of air and moisture-sensitive, zero-valent nickel complex **22** (Scheme 13). Efforts to synthesize compound **22** from the combination of **1** and $Ni(COD)_2$ resulted in suboptimal yield and slower conversion rates. Notably, unlike the case of CAACs, the stoichiometric interaction of BICAACs and $NiBr_2$ formed four-coordinated $[(^{Me}BICAAC)NiBr_2]$ in lower yield and the formation of $[NiBr(\mu\text{-}Br)(BICAAC)]_2$ was not observed.[46] Furthermore, complexes **19–22** were employed for the Negishi cross-coupling reaction of various aryl halides with both fluorinated and non-fluorinated organozinc reagents. These reactions yielded moderate to excellent yields without the use of any additives (Scheme 14).

Mechanistic investigations using UV-Vis studies, HRMS measurements, and controlled stoichiometric reactions provided insights into the catalytic process. Based on the findings, the authors proposed a Ni(I)/Ni(III) catalytic cycle for **19–21**, while a Ni(0)/Ni(II) catalytic cycle was proposed for the Ni(0) complex **22** (Scheme 15). The complex **19** is reusable, stable, and thermally robust and showed the highest catalytic activity among **19–22**.

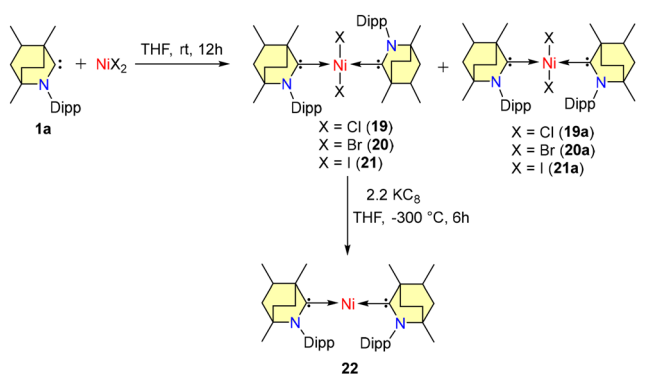

Scheme 13 Synthesis of Ni-BICAAC complexes.

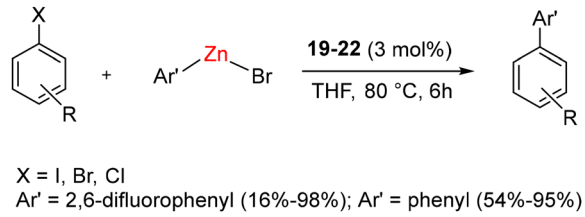

Scheme 14 Negishi cross coupling using **22**.

In the year 2021, Mandal *et al.* reported the synthesis and reactivity of a water stable zero-valent zinc complex $(BICAAC)_2Zn$ (**24**) (Scheme 16).[47a] The process involved the reaction of $BICAAC^{Me}$ (**1a**) with anhydrous zinc chloride in equimolar proportions in toluene at a temperature of 25 °C, resulting in the formation of dimeric complex **23**. Subsequently, this complex was subjected to reduction by KC_8 to form **24** (Scheme 16).

Compound **24** can be stored under an inert atmosphere at room temperature indefinitely. Furthermore, compound **24** is stable in degassed water. However, compound **24** gradually

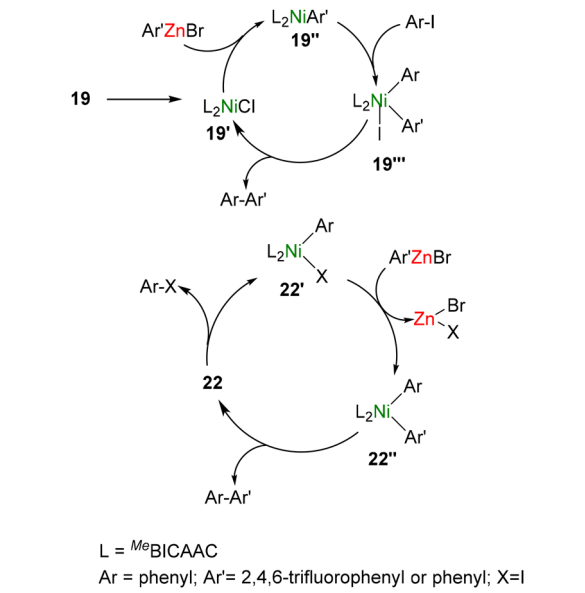

Scheme 15 Mechanistic pathway of Negishi coupling with **19** and **22**.

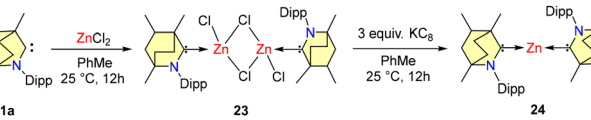

Scheme 16 Synthesis of **23** and **24**.

decomposes into unidentified colorless solids after a few hours of exposure to air.[47a]

The closed shell triplet and singlet states of compound **24** are both more energetic than the singlet biradicaloid state. The ground state spin value being zero is a result of antiferromagnetic interaction, which arises from the weak superexchange between the unpaired electrons situated on the carbene carbon atoms and the filled d-orbitals of zinc (Fig. 4a). Furthermore, the LUMO–SOMO gap of **24** is lower than that of the similar zero valent zinc complex $(CAAC)_2Zn$ (Fig. 4b).[47b]

In contrast to compound **24**, which was unable to activate H_2, $(CAAC)_2Zn$ reacted with H_2 to afford $CAACH_2$ while depositing zinc metal. Compound **24** was capable of forming a zwitterionic adduct **25** upon interaction with CO_2 and can reduce trityl chloride to Gomberg's triphenyl methyl radical much more efficiently than metallic zinc (Scheme 17).

The conversion of non-biodegradable polymers, such as polyethylene (PE), into chemical feedstocks represents a sustainable chemical transformation. The utilization of olefin metathesis within the realm of green chemistry, particularly in the context of sustainable catalysis, is an emerging trend. In 2022, Tuba *et al.* introduced temperature-activated BICAAC-Ru metathesis catalysts that exhibit high selectivity compared to the well-established second-generation Hoveyda–Grubbs and CAAC-Ru catalysts.[48] The synthesis of mono-carbene BICAAC ruthenium complexes **26–29** involves a phosphene–carbene ligand exchange, utilizing *in situ* generated free carbenes **1b–e**, with the first-generation Hoveyda–Grubbs catalyst (**HG1**), as depicted in Scheme 18. Additionally, bis-carbene complexes

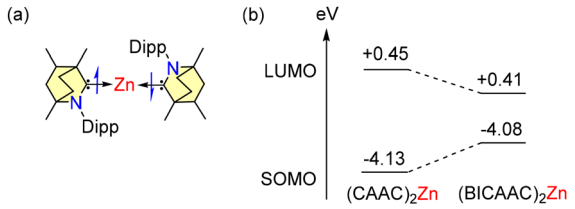

Fig. 4 (a) Singlet biradicaloid state of **24** and (b) LUMO–SOMO gap of $(CAAC)_2Zn$ and $(BICAAC)_2Zn$.

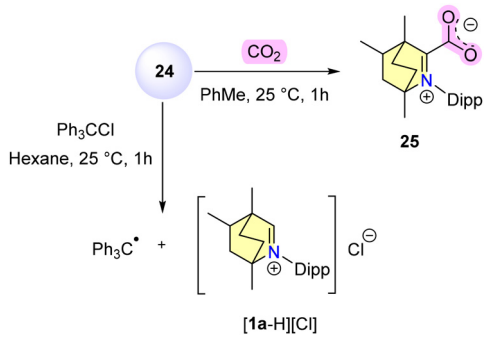

Scheme 17 CO_2 activation and reduction of triphenylmethylchloride with **24**.

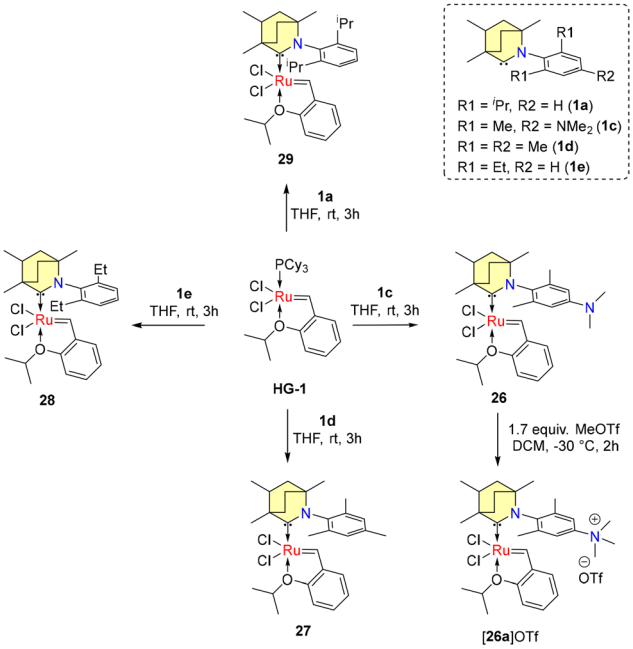

Scheme 18 Synthesis of mono-carbene ruthenium complexes.

30–31 are synthesized using first-generation Grubbs catalysts (**G1**), as outlined in Scheme 19.

While mono-carbene complexes **26–29** are stable in air, the bis-carbene complexes **30–31** can be purified in air but have a shorter shelf-life imparted by the strong *trans*-effect of the BICAAC ligands. The ionic methylated complex **26a**[OTf] could be isolated, while **30a**$[OTf]_2$ was more sensitive. Remarkably high yields were achieved at 75 °C in the context of ring-closing metathesis reactions involving diallyl diethyl malonate with compounds **26–28** as well as **31**. However, no reaction was observed with **26a**[OTf] under similar conditions (Scheme 20a). For the isomerization metathesis reaction of 1-octadecene with **26**/**[RuH]** (as part of a dual catalyst system)

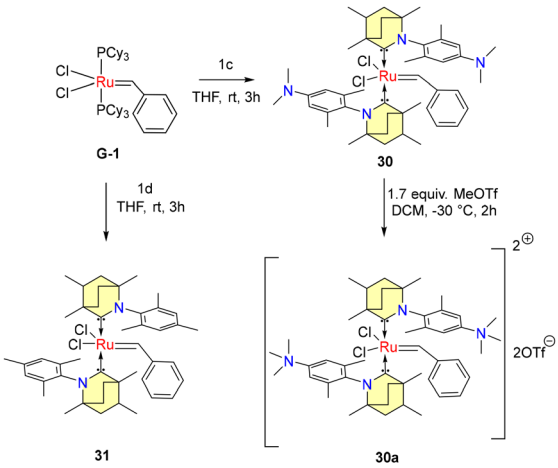

Scheme 19 Synthesis of bis-carbene ruthenium complexes.

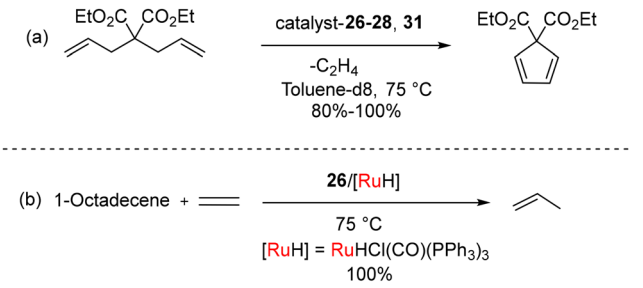

Scheme 20 (a) Ring closing metathesis and (b) ISOMET reactions catalyzed by ruthenium complexes.

in the presence of 99.995% pure ethylene gas, selective production of propylene is achieved with a remarkable turnover number (TON) of 55 000 after a reaction time of 48 hours (Scheme 20b). Later, Turczel *et al.* reported metathesis reactions catalyzed by amberlyst-15/36 supported **26** having efficiency better than CAAC-based systems, as higher yields were obtained at lower catalyst loading.[49]

In 2021, Singh *et al.* reported homogeneous cross-coupling reactions catalyzed by a palladium-BICAAC complex, conducted under open air conditions.[50] The catalyst **32** was synthesized in accordance with Scheme 21.

The activity of the catalyst **32** was found to be better in comparison with tetracyclic-NHC-based palladium complexes. With less catalyst loading, the complex **32** exhibited higher activity than tetracyclic-NHC-based palladium complexes.[51,52]

In the context of Heck–Mizoroki cross-coupling reactions involving aryl bromides featuring electron-withdrawing substituents, the use of catalyst **32** led to impressive yields ranging from 71% to 83%, as illustrated in Scheme 22a.

Moreover, *tert*-butylacrylate and styrene as coupling partners yielded the formation of the respective products.

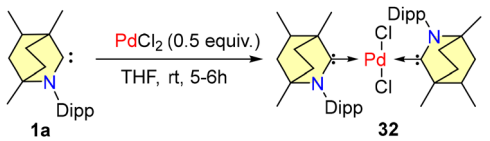

Scheme 21 Synthesis of **32**.

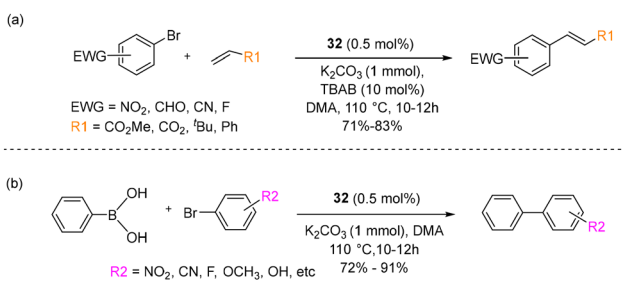

Scheme 22 (a) Heck–Mizoroki and (b) Suzuki–Miyaura cross-coupling reactions using **32**.

Furthermore, they extended their investigation to the activity of the catalyst in Suzuki–Miyaura cross-coupling reactions, as depicted in Scheme 22b. Diverse substrates were explored, including aryl bromides featuring electron-withdrawing groups (EWGs), electron-donating groups (EDGs), and bromofuraldehyde, all yielding substantial yields ranging from 72% to 91%. Notably, following the completion of the reaction, catalyst **32** gradually degrades into inactive palladium nanoparticles. However, the absence of a considerable effect of mercury on the reaction medium suggested the homogeneous nature of the reaction.

Subsequently, in the year 2022, Tuba *et al.* disclosed findings regarding Mizoroki–Heck coupling reactions catalyzed by air and moisture resistant Pd-PEPPSI (PEPPSI = pyridine enhanced precatalyst preparation stabilization and initiation) complexes, supported by BICAAC ligands.[53] Bispyridine-$PdCl_2$ complexes **33a–b** were produced by reacting $PdCl_2$ with pyridine in a 1 : 3 molar ratio in methanol (Scheme 23). The reaction with equimolar amounts of free carbenes and palladium (II)-chloride-bis-pyridine complexes in a 1,4-dioxane medium at 80 °C for 2 hours formed the corresponding PEPPSI complexes (**34a–e**) (Scheme 23).

Crystal structure analysis showed that **34a** and **34b** are crystalized as racemates with *enantio*-pairs in the lattice with square planar coordination around Pd(II). Similar catalytic activity is shown by complexes (**34a–e**) in coupling reactions except for **34c**, which has an isopropyl group adjacent to the carbene carbon atom, which hindered the activity. Moreover, the other substituents of the catalysts did not show any significant impact on efficiency. Coupling of various olefins like styrene, 1-dodecane, 1-octadecene, hepta-1,6-dien-4-ol, and 9-decene-1-ol with substituted aryl bromides yielded excellent conversions (95%–100%). Longer-chain olefins potentially underwent double bond isomerization, possibly catalyzed by intermediate metal hydrides. Poor yields were the result of substrates that were sterically hindered (Scheme 24). Notably, it was discovered that air reduced the catalytic efficiency.

Very recently in 2024, Sanjay Singh and coworkers reported bench-stable BICAAC derived iridium complexes exhibiting remarkable catalytic activity in transfer hydrogenation and hydrosilylation reactions.[54] Complex **35** was synthesized using

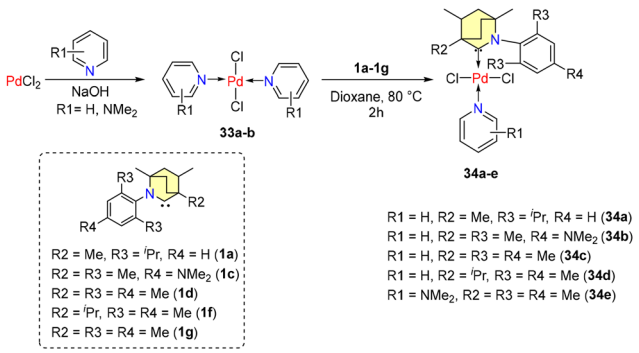

Scheme 23 Synthesis of Pd-PEPPSI complexes.

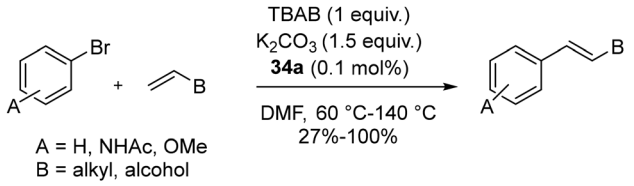

Scheme 24 Mizoroki–Heck coupling catalyzed by **34a**.

0.5 equivalents of $[IrCl(COD)]_2$ along with a free BICAAC (Scheme 25). The synthesized complex (**35**) was further treated with $AgSbF_6$ to generate the corresponding iridium cation (**35a**), which demonstrated reactivity with acetonitrile, a Lewis base, forming the adduct (**35b**) at room temperature (Scheme 25).

Subsequent studies demonstrated that these BICAAC-Ir complexes can function as catalysts for the transfer hydrogenation of aldehydes, ketones, and imines, using ^{i}PrOH as the hydrogen source (Scheme 26).[54] These findings motivated further evaluation of the catalyst's general applicability in hydrosilylation reactions. Both electron-rich and electron-poor aldehydes underwent successful hydrosilylation with Et_3SiH as the reducing agent with catalyst **35**.

5. BICAACs as metal-free catalysts

The first theoretical study on the activation of enthalpically strong bonds by BICAAC ligands was reported by Phukan *et al.* in 2018.[55] It was found that BICAACs can activate N–H bonds *via* either an electrophilic pathway or a nucleophilic pathway. Conversely, the activation of P–H bonds occurs exclusively through a nucleophilic pathway, and Si–H bonds are activated through a hydride transfer pathway.[55]

Tiwari *et al.* conducted computational studies on SO_2 activation by several modelled BICAACs employing Density Functional Theory (DFT) methods.[56] Later in 2019,[57] Koley *et al.* theoretically predicted the electronic nature of carbene–alane and carbene–borane adducts using density functional theory. They reported that $C_{carbene}$–boron bonds are slightly covalent in nature. Notably, the interaction energies, ΔE_{int}, and dissociation energy D_e of the BICAAC·BH_3 adduct surpassed those of all other carbene–borane adducts.

Similar patterns were observed with the BICAAC-AlH_3 adduct as well. In AlH_3 adducts, the electron density of $C_{carbene}$–Al bonds is polarised towards the carbon center. Transition state energy analysis further unveiled that the tendency of BICAACs to form adducts with small boron hydrides, BH_3, and insertion products with more hydridic reagents like B_2Pin was thermodynamically favored.

In 2019, Singh *et al.* reported experimental results on B–H bond activation and borane adduct formation utilizing BICAAC ligands.[58] The synthesis of borane adducts (**36a–g**) was carried out following Scheme 27. Among them, **36a** demonstrated air stability for a limited duration, whereas the other adducts exhibited high sensitivity to moisture and oxygen. Notably, the reaction of a BICAAC with bulky $B(C_6F_5)_3$ produced the BICAAC·$B(C_6F_5)_3$ adduct (**36g**) as the major product. The production of BICAAC-borane adducts, [BICAAC·BH_3] (**36a**), [BICAAC·$BHCl_2$] (**36b**), [BICAAC·BH_2Cl] (**36c**), [BICAAC·BF_3] (**36d**), [BICAAC·BCl_3] (**36e**), and [BICAAC·BBr_3] (**36f**), is consistent with NHC and CAAC findings. However, reactions of the BICAAC with more hydridic

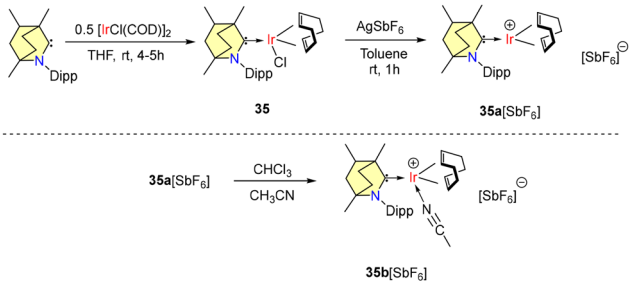

Scheme 25 Synthesis of BICAAC-Ir complexes and their cationic reactivity.

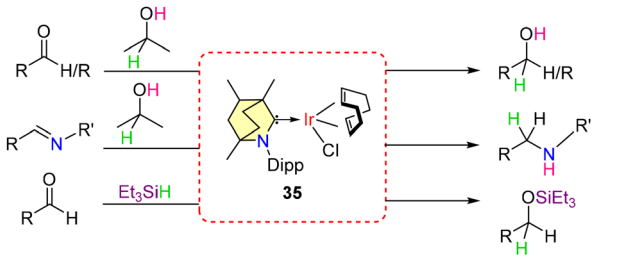

Scheme 26 Transfer hydrogenation and hydrosilylation reactions of complex **35**.

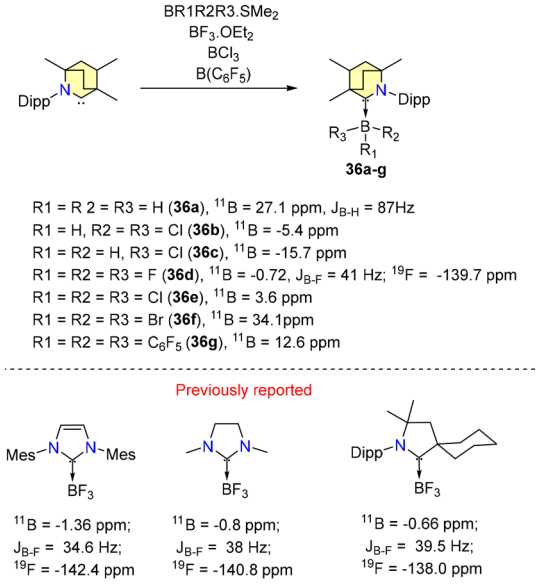

Scheme 27 Synthesis of BICAAC-borane adducts and comparison of the chemical shifts of (carbene)·BF_3 adducts in $^{11}B\{^1H\}$ and $^{19}F\{^1H\}$ NMR.

boranes (9-BBN and catecholborane) that allow the activation of the B–H bond to create [BICAAC(H)-9-BBN] (**37a**) and [BICAAC(H)-Bcat] (**37b**) show that the BICAAC has reactivity akin to CAACs (Scheme 28). This reaction proceeded through the insertion of the carbene's carbon center into the B–H bonds, leading to the formation of air-sensitive complexes **37a** and **37b** (Scheme 28). The boron center has a tetrahedral geometry in **36a–g** and a trigonal planar arrangement in **37a–b**. The thermodynamic viability of adduct and insertion product formation was further substantiated by quantum computational intrinsic reaction coordinate (IRC) calculations. (NHC)·BF_3, (CAAC)BF_3, and (BICAAC)BF_3 showed similar chemical shifts in $^{11}B\{^1H\}$ and $^{19}F\{^1H\}$ NMR (Scheme 24), which did not reflect the electronic and steric properties of the carbenes.[59–61]

Mandal *et al.* reported BICAAC catalyzed silylative dehydration of 2-methyl benzamide to their corresponding nitrile using $PhSiH_3$ as a silylative reagent with a yield of 73% in 12 h (Scheme 29).[62] Interestingly, extending the reaction time (24 h) resulted in a proportional increase in the product yield (86%). Further investigation revealed that NHCs, such as saturated IPr and IPr, demonstrated much reduced catalytic activity (48% and 14%) under identical conditions. The authors noted that the higher nucleophilicity of the BICAAC was essential for the efficiency of this reaction.

In the year 2020, the Bertrand research group unveiled a novel approach for activating CO molecules using a BICAAC and CAAC.[63] Their investigation revealed that when free carbene **1a** reacts with CO in deuterated benzene under ambient conditions, an immediate formation of amino ketene is triggered (Scheme 30). The resulting blue crystals of compound **38** were isolated from dry pentane, with a distinct CO stretching vibration (ν_{str} co) noticeable at 2080 cm^{-1}. Further experimentation showed that compound **38** readily interacts with equimolar amounts of 9,10-phenanthrenequinone (Quin), culminating in the synthesis of spirolactone **39a** with a 74% yield. Subjecting a deuterated benzene solution of **39a** to 4 atm CO at 80 °C produced black residues alongside carbonylated quinone **40** (Scheme 30).

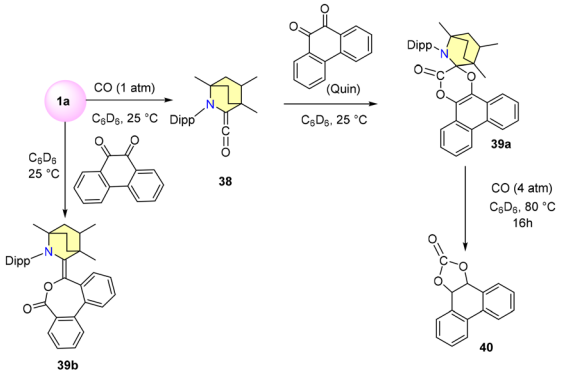

Scheme 30 Reactivity of the (BICAAC)CO adduct.

Additionally, the reaction of **39a** with elemental sulfur (S_8) yielded compounds **39c** and **40**. Intriguingly, the interaction of compound **40** with **1a** regenerated **39a**, thus confirming the reversible nature of the reductive elimination process (Scheme 31). In order to comprehend the mechanism and investigate potential pathways, ethylene carbonate **41** was selected as the desired substrate.[63] At room temperature, it was noted that **1a** readily combines with **41** to form a diastereomeric mixture, specifically a 76 : 24 ratio of **42a** and **42b** (Scheme 32).

This transformation proceeds *via* the intermediates **41a** and **41b**. Interestingly, when the reaction temperature is elevated to 80 °C, the proportion of product formation experiences a reversal, as indicated in Scheme 32. Notably, efforts to employ **1a** as an organic catalyst were unsuccessful, primarily due to the emergence of an inactive adduct **39b** (Scheme 30). The bulky CAAC ligand catalytically facilitated the same carbonylation of an *o*-quinone into a cyclic carbonate.[63]

In another report, Mandal *et al.* have reported BICAAC catalyzed solvent-free, gram-scale reduction of nitriles to amine hydrochloride salts utilizing pinacolborane as the reducing agent.[64] However, the authors did not mention anything on the possibility of hidden boron catalysis.[65]

This approach encompasses a diverse substrate scope, which includes the reduction of electron-donating and with-

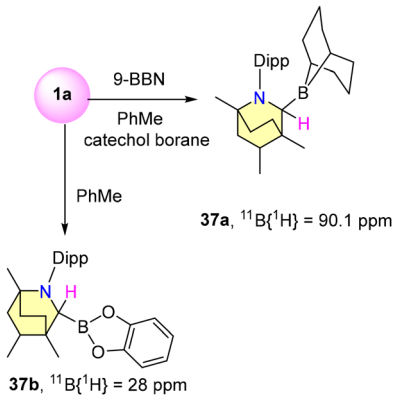

Scheme 28 Formation of B–H insertion products (**37a–b**).

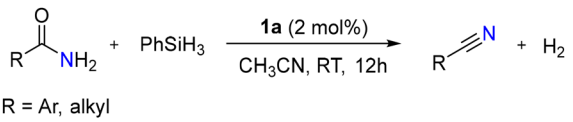

Scheme 29 Silylative dehydration of primary amides to nitriles using **1a**.

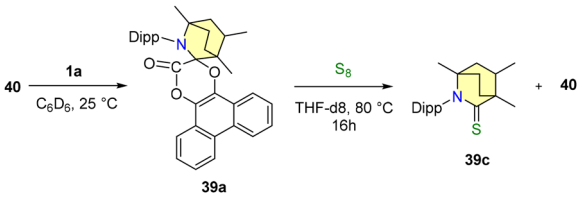

Scheme 31 Reductive elimination at the BICAAC centre.

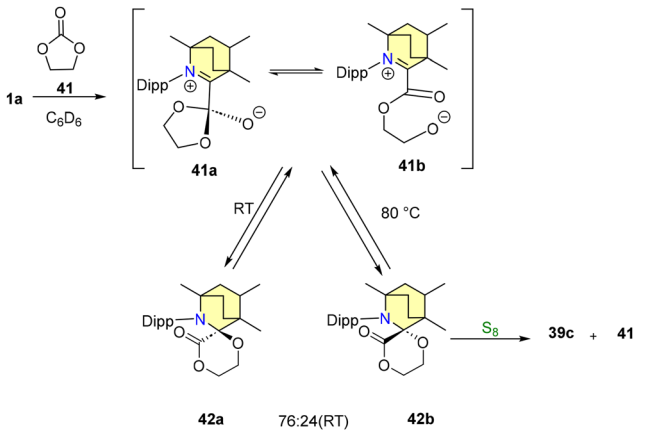

Scheme 32 Formation of 42a–b.

drawing group substituted aromatic nitriles, halogen-substituted benzonitriles, and heterocyclic nitriles, as well as cyclic and acyclic aliphatic nitriles, with moderate to good yields (Scheme 33). However, the observations reflect that *ortho*-substituted benzonitriles afforded unsatisfactory yields. Mechanistic insights revealed that the B–H insertion product **43** serves as a hydride donor during the reduction process (Scheme 34). This intermediate formation was validated through computational analyses and deuterium labelled (DBPin) experiments (Scheme 34). Similar results have also been reported by Sen *et al.* in 2022 using a six-membered NHC, which also supports this insertion reaction.[66]

In another report, Mandal *et al.* demonstrated a BICAAC as a catalyst for the *N*-methylation of primary amides using CO_2 as the carbon source and H-Bpin as the reducing agent.[67] The reaction exhibited robust tolerance towards various amides containing electron-donating, electron-rich, and heterocyclic groups, as well as biologically active molecules with amide moieties (Scheme 35).

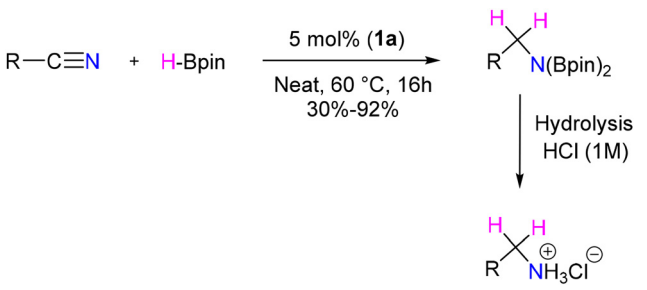

Scheme 33 BICAAC catalyzed reduction of nitriles.

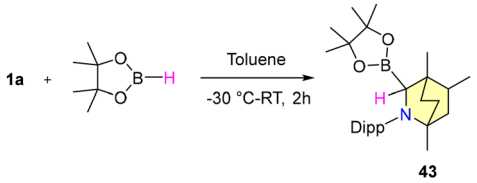

Scheme 34 Reaction of HBpin with a BICAAC.

Mechanistic investigations have unveiled that the insertion product **43** and the adduct **45** possess the capability to catalyze *N*-methylation, likely attributable to their interconversion and the potential formation of intermediate **47** (Scheme 36). The role of **43** involves activating the amide bonds to generate *N*-borylated amide **48**. On the other hand, adduct **45** interacts with H-Bpin, undergoing hydride transfer to establish transition state **46**, which subsequently evolves into intermediate **47**. The progression of **47** leads to the formation of *N*-borylated acetamide **49**, followed by consecutive transformations resulting in aminal **51** and **50** $(Bpin)_2O$. The transformation continues as **51** is further subjected to reduction by H-Bpin, ultimately yielding the desired *N*-methylated amide **52** (Scheme 36). The proposed catalytic cycle pathway finds support through controlled experiments.

In 2024, Singh and coworkers exploited the ambiphilic properties of the BICAAC for the dehydrogenation of alcohols and it was reported that the activation pathway closely resembles the conventional metal–ligand cooperative activation of a substrate (Scheme 37a).

A stoichiometric reaction of benzyl alcohol and a BICAAC at 60 °C resulted in the formation of $(BICAAC)H_2$ (**54**) and benzaldehyde in 60% yield (Scheme 37a).[68] Furthermore, they have

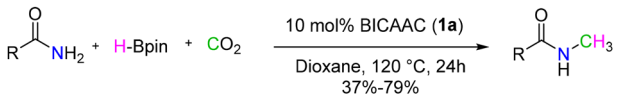

Scheme 35 *N*-Methylation of primary amides.

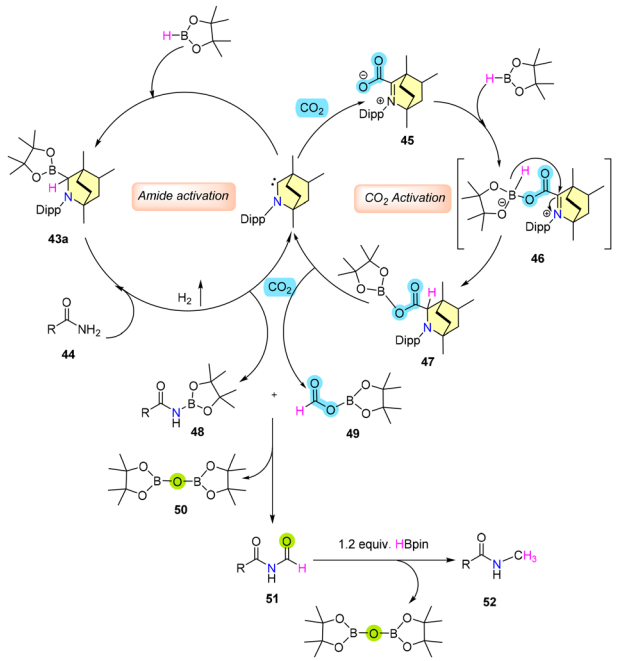

Scheme 36 Mechanistic pathway for *N*-methylation of primary amides.

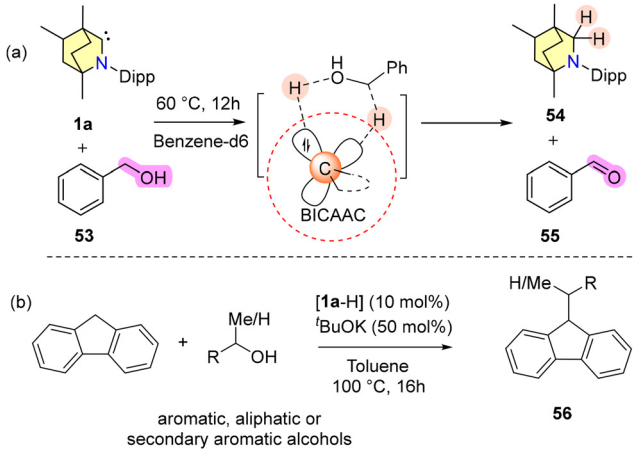

Scheme 37 (a) Dehydrogenation of alcohol using a BICAAC through the ambiphilic action of the BICAAC and (b) BICAAC catalysed fluorene alkylation.

used a BICAAC as a catalyst for the alkylation of fluorene at its 9-position using various alcohols as the alkyl source (Scheme 37b).

6. BICAAC-supported main-group compounds

In 2023, our group reported water and air-stable glyoxal radicals stabilised by a BICAAC (Scheme 38a).[69] The synthesis of the radical **57**[BF_4] is given in Scheme 38. Interestingly, **57**[BF_4] was found to be stable under acidic and basic conditions as well as in H_2O_2, thiophenol and bovine serum. **57**[BF_4] showed excellent thermal stability (stable up to 200 °C). Notably, UV spectral analysis indicated that the BICAAC stabilized radical cation **57**[BF_4] exhibited stability towards acids and bases (Scheme 38b).[69a] Similar glyoxal radical ions were also reported with NHC ligands by Lee *et al.* in 2021 (Scheme 38b).[69b]

The DFT study revealed that the spin density of **57** has been delocalised over the central glyoxal unit, along with negligible contributions from the carbene groups.

Furthermore, cyclic-voltammetric investigations exhibited reversible one-electron oxidation and reduction phenomena of **57**[BF_4], which were verified by chemical synthesis (Scheme 38a).

In 2024, Mandal *et al.* carried out an extensive electrochemical study of compound **57**[BF_4] using cyclic voltammetric techniques.[70] Based on the outcome of this study, they proposed its potential application in symmetric H-cell cycling (Scheme 39).[70]

Sanjay Singh and co-workers in 2024 demonstrated that reacting BH_2Cl and KC_8 in the presence of a free BICAAC affords diborane complex **60** (Scheme 40).[71a] Similarly, a reaction of $BHCl_2$ and 2 equiv. of KC_8 in the presence of a BICAAC affords diborene **61** (Scheme 40).[71a] Both **60** and **61** are highly sensitive to air and moisture. Compound **60** exhibits a signal at $\delta = -16.4$ ppm in $^{11}B\{^1H\}$ NMR spectroscopy, whereas it is further downfield shifted in **61** at 42.6 ppm. The ^1H NMR spectrum displays a broad signal at 5 ppm corresponding to the BH protons of **61**. The frontier molecular orbital diagram ana-

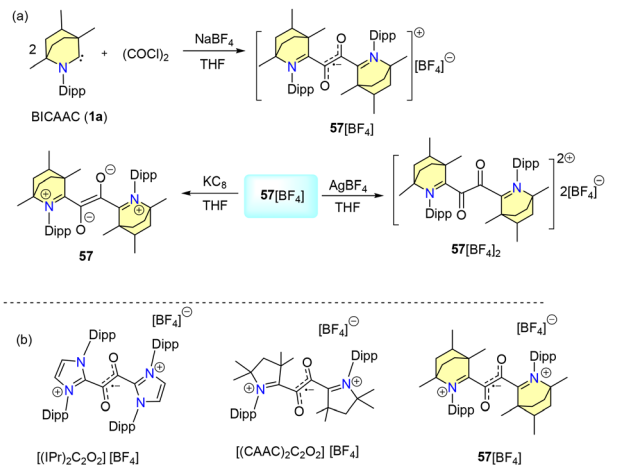

Scheme 38 (a) Synthesis of a glyoxal radical cation using a BICAAC. (b) Examples of related radical ions.

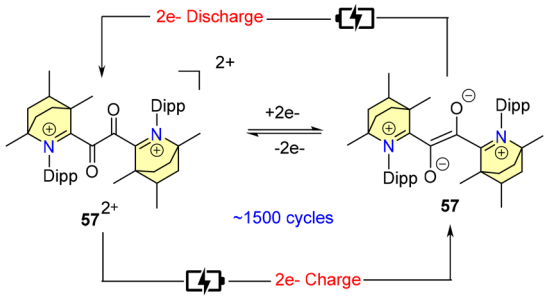

Scheme 39 Schematic representation of symmetric H-cell cycling based on **57**[BF_4].

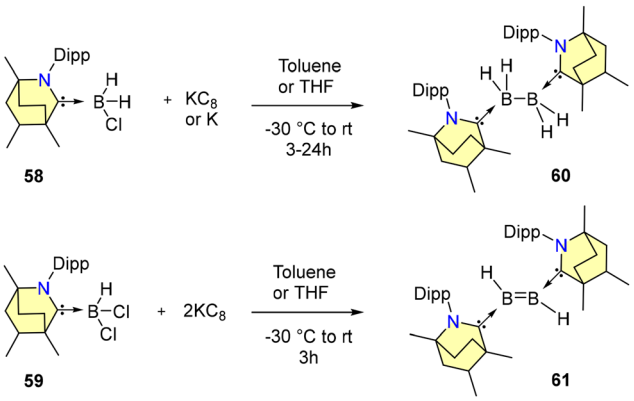

Scheme 40 Synthesis of BICAAC-diborane (**60**) and diborene (**61**) complexes.

lysis indicates that diborene **61** has the lowest HOMO–LUMO gap in comparison with its NHC analogue.[71b]

The diborene **61** forms complexes with coinage metal halides (CuCl, AgBr, and CuI) (Scheme 41). It was observed that B=B coordinated to two units of CuCl in a η^2-coordination mode (**62**). In contrast, η^1-coordinating complexes of Ag and Cu were formed when **61** was reacted with AgBr and CuI, yielding solid compounds **63** and **64**, respectively. Compound **63** remains stable under inert conditions and below −15 °C.

Only a few BICAAC complexes of heavier main group elements have been reported to date. Among them, very recently, Singh and co-workers reported the synthesis of low-valent stable silicon complexes (**65–68**) derived from BICAACs and Si(IV) precursors (Schemes 42 and 43).[72] Starting with 1 equiv. of $SiCl_4$ and a free BICAAC, compound **65** was synthesised with a yield of 76% (Scheme 42). Compound **65** exhibited a highly upfield-shifted signal at −106.8 ppm in the ^{29}Si NMR spectrum, compared to its precursor ($SiCl_4$ = −18 ppm). (^{Me}BICAAC)$SiCl_4$ (**65**) was thermally stable up to 196–198 °C.

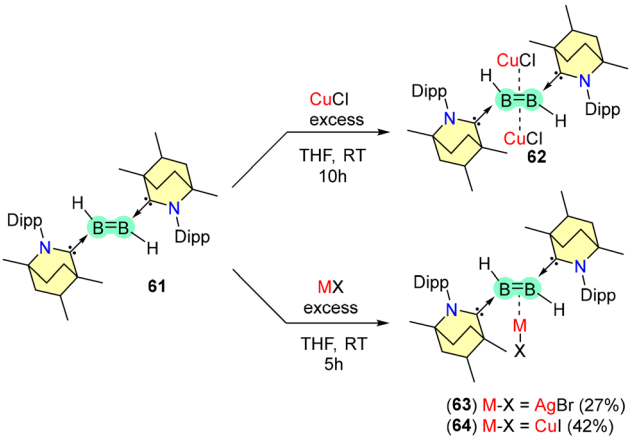

Scheme 41 Coinage metal complexes of BICAAC-diborene.

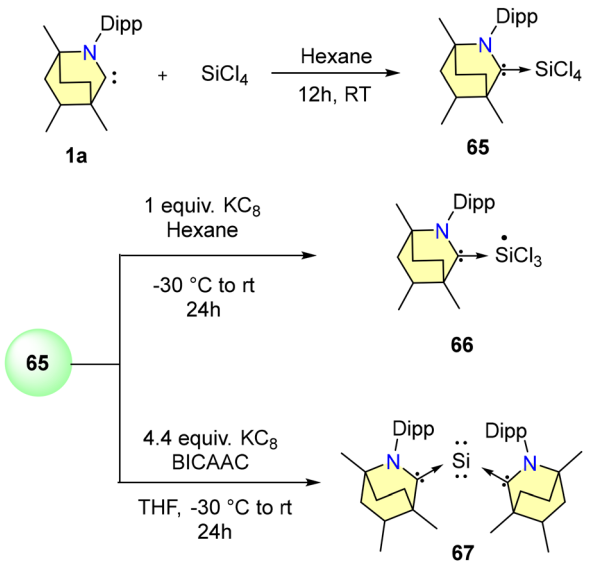

Scheme 42 Synthesis of BICAAC stabilised low-valent silicon compounds.

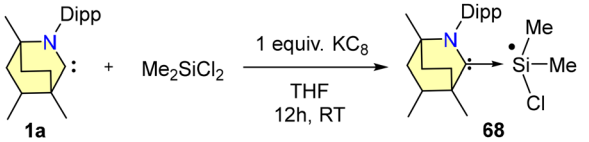

Scheme 43 Synthesis of a BICAAC-Si(III) radical.

The reduction of **65** with either one equivalent or an excess of KC_8 produced **66** and **67**, respectively (Scheme 42). Compound **66** is a mono-radical and the formal oxidation state of silicon is +3. **67** is a bent, two-coordinated Si(0) compound. Furthermore, the singlet ground state and silylone nature of complex **67** were supported by DFT calculations. From SCXRD techniques, it was revealed that the Si(0) adopts a bent geometry and is coordinated with two BICAAC units in the monoclinic system with a *C*2/*c* space group. Additionally, Si(III) radical **68** was also formed *via* a single-pot reaction of Me_2SiCl_2 with a BICAAC and KC_8 in THF (Scheme 43). It was isolated with a yield of 73% as an orange-red solid.

Bertrand *et al.*, in their 1st report of isolating BICAACs, synthesized selenium and phosphinidene adducts [(^{Me}BICAAC)Se (**69**) and (^{Me}BICAAC)PPh (**70**)] of ^{Me}BICAAC (**1a**) to study the electronic properties of BICAACs (Scheme 39).[9] The ^{31}P{^{1}H} NMR signal displayed a remarkable shift to +90 ppm for compound **70**, diverging from the +56 to +69 ppm range seen in CAACs.[73] Similarly, the ^{77}Se NMR spectrum of compound **69** revealed a distinctively downfield signal at +645 ppm, in stark contrast to +492 ppm and +87 ppm exhibited by (^{Me2}CAAC)Se and (IPr)Se, respectively.[74,75] This pronounced shift highlighted the better π-accepting and σ-donating capabilities inherent to BICAACs compared to their CAAC counterparts. Furthermore, treating **1a** with dibromine forms bromide salt **71** (Scheme 44).

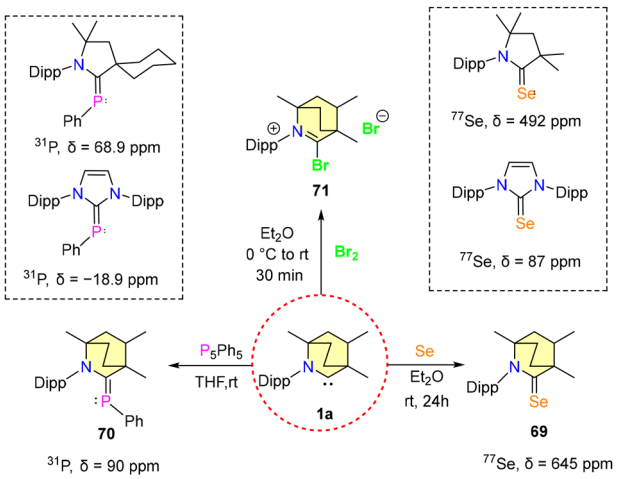

Scheme 44 Reactivity of **1a** towards Se, P_5Ph_5 and Br_2.

In 2023, Singh *et al.* reported the synthesis of (BICAAC)ECl_3 adducts (E = P, **72** and Sb, **73**) and their three-electron reduction to form $(BICAAC)_2E_2$ (E = P, **74** and Sb, **75**) complexes (Schemes 45 and 46).[76] The single crystal X-ray analysis revealed that P and Sb have seesaw geometry in compounds **72–73**. The $^{31}P\{^1H\}$ NMR of (BICAAC)PCl_3 (**72**) showed a single peak at 33.0 ppm, whereas the compound $(BICAAC)_2P_2$ (**74**) showed two closely spaced singlets of equal intensity at 65.5 and 65.3 pm (due to two diastereomers). The $^{31}P\{^1H\}$ signal of **74** stands relatively deshielded compared to its corresponding NHC analogue, specifically the $(IPr)_2P_2$ compound (δ = −52.4 ppm) (Scheme 41).[77] The corresponding $(^{cy}CAAC)_2P_2$ shows the $^{31}P\{^1H\}$ signal at 59.4 ppm.[78] This distinctive shift is attributed to the increased electrophilicity of the BICAAC carbene. The $C_{carbene}$–P bond distance in **74** [1.734(14) Å] was found to be shorter when compared with the $C_{carbene}$–P bond distance in $(IPr)_2P_2$ [1.7504(17) Å] and comparable with the $C_{carbene}$–P bond length of $(^{cy}CAAC)_2P_2$ [1.719(7) Å] (Scheme 41). Meanwhile, the P–P bond distance in **74** [2.203(6) Å] is comparable with the P–P single bond distance of molecular tetrahedral P_4 (2.21 Å) and also comparable with that of $(IPr)_2P_2$ [2.2052(10) Å] and $(^{cy}CAAC)_2P_2$ [2.184(3) Å] (Scheme 41).[77,78] The experimental data indicate that the bis(phosphinidene) (**74**) is better represented as bis(phosphaalkene), whereas the antimony analogue (**75**) is described as a BICAAC stabilized Sb_2 core.

In 2023, our group reported the synthesis of BICAAC stabilised halophosphaalkenes (**76–78**), which were obtained by reacting free BICAACs with PX_3 (X, X = Cl, Br, and I) in THF, as shown in Scheme 47.[79] Compounds **76–78** were characterized

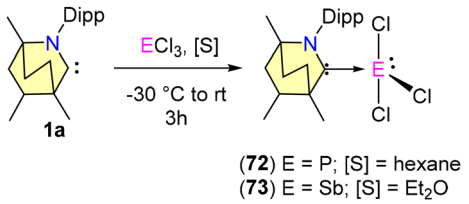

Scheme 45 Synthesis of (BICAAC)ECl_3 adducts (E = P and Sb).

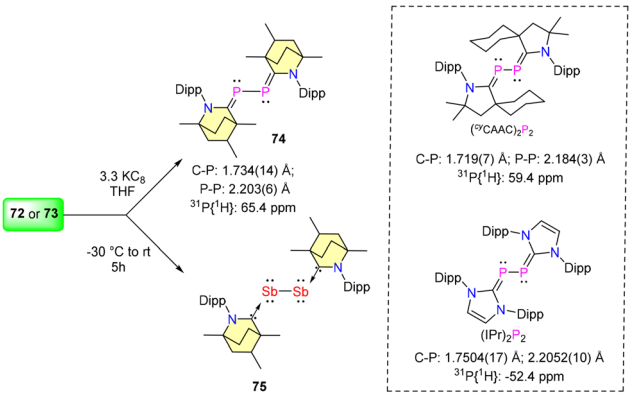

Scheme 46 Synthesis and comparison of $(BICAAC)_2E_2$ complexes.

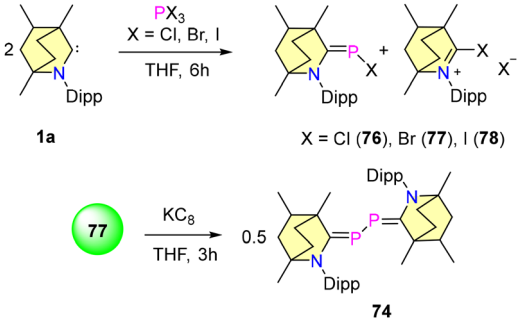

Scheme 47 Synthesis of BICAAC stabilized halophosphaalkenes and bisphosphinidenes.

by single crystal XRD techniques and heteronuclear NMR spectroscopy. The $^{31}P\{^1H\}$ studies revealed that compound **76** shows a downfield shift at 115.35 ppm compared to **77** (103.12 ppm) and **78** (56.13 ppm), and this is mainly due to the electronegativity differences between halogens. Furthermore, the reduction of compound **77** with 1 equiv. of KC_8 resulted in the formation of **74**. Note that compound **74** can also be synthesized from the direct reduction of (BICAAC)PCl_3 as discussed (*vide supra*).[76] There have been several reports where NHC and CAACs have been used as supporting backbone ligands for the isolation of phosphenium cations, but none have been found to show air and moisture stability.[80–83] Recently, our group employed a BICAAC for the isolation of an air- and water-stable phosphenium cation **78**.[84] [(BICAAC)PPh_2]OTf was obtained in good yields from the reaction of the BICAAC with Ph_2PCl in THF, followed by ion exchange with LiOTf. The increased π-accepting properties of the BICAAC have been reflected by $^{31}P\{^1H\}$ NMR spectroscopic data, as compound **78** exhibits a singlet peak at +13.73 ppm, which is downfield shifted in comparison with its NHC[85,86] [$(^{Me2}Im)P(Ph)_2$][PF_6] ($^{31}P\{^1H\}$ = −25.89 ppm) and CAAC[82,83] [$(^{Me2}CAAC)P(Ph)_2$][SbF_6] ($^{31}P\{^1H\}$ = 0 ppm) analogues. Furthermore, the cyclic voltammogram of **78** showed one electron reversible

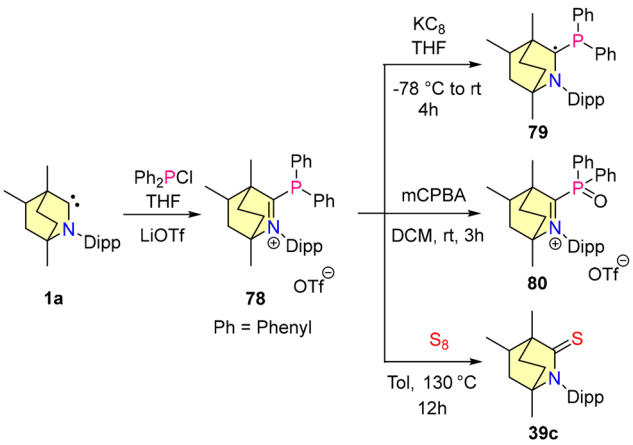

Scheme 48 Synthesis of a BICAAC stabilized phosphenium cation (**78**) and its reactivity.

redox process. The reduction of **78** with 1 equiv. of KC_8 resulted in the formation of radical phosphine **79**. Moreover, the oxidation of **78** using *m*CPBA yielded **80**, which proved the oxophilic nature of phosphorus (Scheme 48). Remarkably, complex **78** showed selective binding to fluoride ions and no interaction with other halides (Cl^- and Br^-) was observed.

7. Conclusions

This review focuses on the synthesis and properties of BICAACs, their usefulness in the synthesis of metal complexes, their applications as metal-free catalysts, and their role in the isolation of low-valent main-group compounds. The decreased HOMO–LUMO gap of BICAACs, combined with their exceptional nucleophilic and electrophilic nature and a unique steric environment due to the bicyclic backbone, makes them distinctive ligands. This is exemplified by the isolation of air- and moisture-stable radicals and phosphenium cations using BICAACs. Additionally, BICAACs have shown promise in the field of metal-free catalysis. BICAAC-coinage metal amides exhibit superior photoluminescence properties and quantum yields compared to CAACs and NHCs, likely due to the system's rigidity, which reduces various vibrational relaxation processes of the excited photoelectrons.

Compared to NHCs and five-membered CAACs, the chemistry of BICAACs has been less explored, possibly due to their relatively recent introduction to carbene chemistry. Therefore, there is significant potential for further investigation. For instance, the chemistry of s-block elements with BICAACs remains largely unexplored. Similarly, there are few examples of stable organic radicals and main-group radicals with BICAACs, and no reports of BICAAC-supported Al, Sn, or Bi complexes. Furthermore, the functionalization of BICAACs to create chelating ligands has not been attempted, although the related chemistry of NHCs is well established. The metal-mimicking metal-free catalysis of BICAACs is also in its infancy but holds great promise for further exploration. Due to its chiral structure, BICAACs can be envisioned for applications relevant to chirality (akin to CAACs).[87] Moreover, theoretical advances in this area could encourage experimental chemists to explore their chemistry. In conclusion, the field of carbene chemistry is undergoing rapid expansion, with the isolation of numerous exotic and previously unattainable species, and we believe that BICAACs will make significant contributions to this domain.

Author contributions

All the authors contributed to writing the manuscript.

Data availability

No primary research results, software or code have been included and no new data were generated or analysed as part of this review.

Conflicts of interest

There are no conflicts to declare.

Acknowledgements

This work was supported by SERB, New Delhi, India (CRG/2023/002353), CSIR, India (01/3041/21/EMR-II) and ASHOKA-IITD MFIRP. Ankita thanks PMRF for the financial support and fellowship. We thank CRF, IIT Delhi for the synthesis lab facility.

References

1 A. Igau, H. Grutzmacher, A. Baceiredo and G. Bertrand, *J. Am. Chem. Soc.*, 1988, **110**, 6463.
2 A. J. Arduengo, R. L. Harlow and M. Kline, *J. Am. Chem. Soc.*, 1991, **113**, 361–363.
3 (*a*) P. R. Sultane, G. Ahumada, D. Janssen-Müller and C. W. Bielawski, *Angew. Chem., Int. Ed.*, 2019, **58**, 16320–16325; (*b*) S. Appel, P. Brüggemann and C. Ganter, *Chem. Commun.*, 2020, **56**, 9020–9023; (*c*) H. Kim, M. Kim, H. Song and E. Lee, *Chem. – Eur. J.*, 2021, **27**, 3849–3854; (*d*) M. Kim, H. Kim, S. Kim, S. Hong and E. Lee, *Organometallics*, 2022, **41**, 1905–1910; (*e*) J. Volk, M. Heinz, M. Leibold, C. Bruhn, T. Bens, B. Sarkar, M. C. Holthausen and U. Siemeling, *Chem. Commun.*, 2022, **58**, 10396–10399; (*f*) S. Solé, H. Gornitzka, W. W. Schoeller, D. Bourissou and G. Bertrand, *Science*, 2001, **292**, 1901–1903; (*g*) D. Magis, J. J. Cabrera-Trujillo, J. Vignolle, J.-M. Sotiropoulos, D. Taton, K. Miqueu and Y. Landais, *J. Am. Chem. Soc.*, 2024, **146**, 16802–16813; (*h*) Y. K. Loh, M. Melaimi, D. Munz and G. Bertrand, *J. Am. Chem. Soc.*, 2023, **145**, 2064–2069.
4 (*a*) S. P. Nolan, *N-Heterocyclic Carbenes*, Wiley-VCH Verlag GmbH & Co. KGaA, 2014; (*b*) H. V. Huynh, *The Organometallic Chemistry of N-Heterocyclic Carbenes*, John Wiley & Sons, Ltd, Chichester, UK, 2017; (*c*) N. I. Korotkikh, G. F. Rayenko, O. P. Shvaika, T. M. Pekhtereva, A. H. Cowley, J. N. Jones and C. L. B. Macdonald, *J. Org. Chem.*, 2003, **68**, 5762–5765; (*d*) D. J. Nelson and S. P. Nolan, *Chem. Soc. Rev.*, 2013, **42**, 6723–6753; (*e*) H. V. Huynh, *Chem. Rev.*, 2018, **118**, 9457–9492; (*f*) P. W. Antoni, C. Golz, J. J. Holstein, D. A. Pantazis and M. M. Hansmann, *Nat. Chem.*, 2021, **13**, 587–593.
5 C. A. Smith, M. R. Narouz, P. A. Lummis, I. Singh, A. Nazemi, C.-H. Li and C. M. Crudden, *Chem. Rev.*, 2019, **119**, 4986–5056.
6 L. Oehninger, R. Rubbiani and I. Ott, *Dalton Trans.*, 2013, **42**, 3269–3284.
7 V. Lavallo, Y. Canac, C. Präsang, B. Donnadieu and G. Bertrand, *Angew. Chem., Int. Ed.*, 2005, **44**, 5705–5709.
8 (*a*) B. Rao, H. Tang, X. Zeng, L. L. Liu, M. Melaimi and G. Bertrand, *Angew. Chem., Int. Ed.*, 2015, **54**, 14915–14919;

(*b*) M. Melaimi, R. Jazzar, M. Soleilhavoup and G. Bertrand, *Angew. Chem., Int. Ed.*, 2017, **56**, 10046–10068.
9 E. Tomas-Mendivil, M. M. Hansmann, C. M. Weinstein, R. Jazzar, M. Melaimi and G. Bertrand, *J. Am. Chem. Soc.*, 2017, **139**, 7753–7756.
10 C. M. Weinstein, G. P. Junor, D. R. Tolentino, R. Jazzar, M. Melaimi and G. Bertrand, *J. Am. Chem. Soc.*, 2018, **140**, 9255–9260.
11 K. Powers, C. Hering-Junghans, R. McDonald, M. J. Ferguson and E. Rivard, *Polyhedron*, 2016, **108**, 8–14.
12 K. Denk, P. Sirsch and W. A. Herrmann, *J. Organomet. Chem.*, 2002, **649**, 219–224.
13 K. C. Mondal, B. Dittrich, B. Maity, D. Koley and H. W. Roesky, *J. Am. Chem. Soc.*, 2014, **136**, 9568–9571.
14 R. W. Alder, P. R. Allen, M. Murray and A. G. Orpen, *Angew. Chem., Int. Ed. Engl.*, 1996, **35**, 1121–1123.
15 F. Vermersch, S. Yazdani, G. P. Junor, D. B. Grotjahn, R. Jazzar and G. Bertrand, *Angew. Chem., Int. Ed.*, 2021, **60**, 27253–27257.
16 O. Back, M. Henry-Ellinger, C. D. Martin, D. Martin and G. Bertrand, *Angew. Chem., Int. Ed.*, 2013, **52**, 2939–2943.
17 K. Verlinden, H. Buhl, W. Frank and C. Ganter, *Eur. J. Inorg. Chem.*, 2015, **2015**, 2416–2425.
18 K. C. Mondal, S. Roy, B. Maity, D. Koley and H. W. Roesky, *Inorg. Chem.*, 2016, **55**, 163–169.
19 (*a*) E. A. LaPierre, L. K. Watanabe, B. O. Patrick, J. M. Rawson, H. M. Tuononen and I. Manners, *J. Am. Chem. Soc.*, 2023, **145**, 9223–9232; (*b*) B. Li, S. Kundu, A. C. Stückl, H. Zhu, H. Keil, R. Herbst-Irmer, D. Stalke, B. Schwederski, W. Kaim, D. M. Andrada, G. Frenking and H. W. Roesky, *Angew. Chem., Int. Ed.*, 2016, **56**, 397–400; (*c*) B. Das, A. Makol and S. Kundu, *Dalton Trans.*, 2022, **51**, 12404–12426; (*d*) J. E. Walley and R. J. Gilliard Jr, Encyclopedia of Inorganic and Bioinorganic Chemistry, 2021, pp. 1–14; (*e*) M.-A. Légaré, M. Rang, G. Bélanger-Chabot, J. I. Schweizer, I. Krummenacher, R. Bertermann, M. Arrowsmith, M. C. Holthausen and H. Braunschweig, *Science*, 2019, **363**, 1329–1332; (*f*) M.-A. Légaré, C. Pranckevicius and H. Braunschweig, *Chem. Rev.*, 2019, **119**, 8231–8261; (*g*) M. Arrowsmith, H. Braunschweig, M. A. Celik, T. Dellermann, R. D. Dewhurst, W. C. Ewing, K. Hammond, T. Kramer, I. Krummenacher, J. Mies, K. Radacki and J. K. Schuster, *Nat. Chem.*, 2016, **8**, 890–894; (*h*) A. Maiti, J. Stubbe, N. I. Neuman, P. Kalita, P. Duari, C. Schulzke, V. Chandrasekhar, B. Sarkar and A. Jana, *Angew. Chem., Int. Ed.*, 2020, **59**, 6729–6734; (*i*) S. A. Gonsales, Z. C. Mueller, F. Zhao, P. H. S. Paioti, L. Karmazin, J. Wan, F. Liu, K. N. Houk and A. H. Hoveyda, *J. Am. Chem. Soc.*, 2021, **143**, 20640–20644; (*j*) V. M. Marx, A. H. Sullivan, M. Melaimi, S. C. Virgil, B. K. Keitz, D. S. Weinberger, G. Bertrand and R. H. Grubbs, *Angew. Chem., Int. Ed.*, 2014, **54**, 1919–1923; (*k*) R. K. Singh, T. K. Khan, S. Misra and A. K. Singh, *J. Organomet. Chem.*, 2021, **956**, 122133.
20 S. Kang, S. E. Byeon and H. J. Yoon, *Bull. Korean Chem. Soc.*, 2021, **42**, 712–723.
21 H. Song, E. Pietrasiak and E. Lee, *Acc. Chem. Res.*, 2022, **55**, 2213–2223.
22 S. K. Kushvaha, A. Mishra, H. W. Roesky and K. C. Mondal, *Chem. Asian J.*, 2022, **17**(7), e202101301.
23 A. Tyagi, S. Mondal, Anmol, V. Tiwari, T. Karmakar and S. Kundu, *Chem. Commun.*, 2023, **59**, 110–113.
24 (*a*) S. Roy, K. C. Mondal and H. W. Roesky, *Acc. Chem. Res.*, 2016, **49**, 357–369; (*b*) M.-M. Li, X. Chen, Y. Deng and J. Lu, *RSC Adv.*, 2021, **11**, 38060–38078; (*c*) K. C. Mondal, S. Roy and H. W. Roesky, *Chem. Soc. Rev.*, 2016, **45**, 1080–1111.
25 (*a*) Y. Pan, X. Jiang, Y.-M. So, C. T. To and G. He, *Catalysts*, 2020, **10**, 71; (*b*) E. Peris, *Chem. Rev.*, 2017, **118**, 9988–10031.
26 R. Jazzar, M. Soleilhavoup and G. Bertrand, *Chem. Rev.*, 2020, **120**, 4141–4168.
27 N. V. Tzouras, E. A. Martynova, X. Ma, T. Scattolin, B. Hupp, H. Busen, M. Saab, Z. Zhang, L. Falivene, G. Pisanò, K. Van Hecke, L. Cavallo, C. S. J. Cazin, A. Steffen and S. P. Nolan, *Chem. – Eur. J.*, 2021, **27**, 11904–11911.
28 S. Kundu, S. Sinhababu, V. Chandrasekhar and H. W. Roesky, *Chem. Sci.*, 2019, **10**, 4727–4741.
29 (*a*) P. Bellotti, M. Koy, M. N. Hopkinson and F. Glorius, *Nat. Rev. Chem.*, 2021, **5**, 711–725; (*b*) R. Yadav, S. Sinhababu, R. Yadav and S. Kundu, *Dalton Trans.*, 2022, **51**, 2170–2202.
30 (*a*) M. Melaimi, M. Soleilhavoup and G. Bertrand, *Angew. Chem., Int. Ed.*, 2010, **49**, 8810–8849; (*b*) S. Kuwata and F. E. Hahn, *Chem. Rev.*, 2018, **118**, 9642–9677.
31 M. Soleilhavoup and G. Bertrand, *Acc. Chem. Res.*, 2015, **48**, 256–266.
32 D. Bourissou, O. Guerret, F. P. Gabbaï and G. Bertrand, *Chem. Rev.*, 2000, **100**, 39–92.
33 D. Magis, J. J. Cabrera-Trujillo, J. Vignolle, J.-M. Sotiropoulos, D. Taton, K. Miqueu and Y. Landais, *J. Am. Chem. Soc.*, 2024, **146**, 16802–16813.
34 (*a*) S. Nayak and S. L. Gaonkar, *ChemMedChem*, 2021, **16**, 1360–1390; (*b*) M. Marinelli, C. Santini and M. Pellei, *Curr. Top. Med. Chem.*, 2016, **16**, 2995–3017; (*c*) M. Mora, M. C. Gimeno and R. Visbal, *Chem. Soc. Rev.*, 2019, **48**, 447–462; (*d*) R. Visbal and M. C. Gimeno, *Chem. Soc. Rev.*, 2014, **43**, 3551–3574; (*e*) J. Hossain, R. Akhtar and S. Khan, *Polyhedron*, 2021, **201**, 115151.
35 J. C. Y. Lin, R. T. W. Huang, C. S. Lee, A. Bhattacharyya, W. S. Hwang and I. J. B. Lin, *Chem. Rev.*, 2009, **109**, 3561–3598.
36 D. Pichon, M. Soleilhavoup, J. Morvan, G. P. Junor, T. Vives, C. Crévisy, V. Lavallo, J.-M. Campagne, M. Mauduit, R. Jazzar and G. Bertrand, *Chem. Sci.*, 2019, **10**, 7807–7811.
37 J. Chu, D. Munz, R. Jazzar, M. Melaimi and G. Bertrand, *J. Am. Chem. Soc.*, 2016, **138**, 7884–7887.
38 (*a*) K. K. Manar, S. Chakrabortty, V. K. Porwal, D. Prakash, S. K. Thakur, A. R. Choudhury and S. Singh, *ChemistrySelect*, 2020, **5**, 9900–9907; (*b*) G. D. Frey, R. D. Dewhurst, S. Kousar, B. Donnadieu and G. Bertrand, *J. Organomet. Chem.*, 2008, **693**, 1674–1682.
39 E. A. Romero, T. Zhao, R. Nakano, X. Hu, Y. Wu, R. Jazzar and G. Bertrand, *Nat. Catal.*, 2018, **1**, 743–747.

40 (*a*) F. Chotard, V. Sivchik, M. Linnolahti, M. Bochmann and A. S. Romanov, *Chem. Mater.*, 2020, **32**, 6114–6122; (*b*) A. S. Romanov, S. T. E. Jones, L. Yang, P. J. Conaghan, D. Di, M. Linnolahti, D. Credgington and M. Bochmann, *Adv. Opt. Mater.*, 2018, **6**, 1801347.
41 X.-F. Song, Z.-W. Li, W.-K. Chen, Y.-J. Gao and G. Cui, *Inorg. Chem.*, 2022, **61**, 7673–7681.
42 Y. Gao, S. Yazdani, A. Kendrick, G. P. Junor, T. Kang, D. B. Grotjahn, G. Bertrand, R. Jazzar and K. M. Engle, *Angew. Chem., Int. Ed.*, 2021, **60**, 19871–19878.
43 Y. Gao, N. Kim, S. D. Mendoza, S. Yazdani, A. F. Vieira, M. Liu, A. Kendrick, D. B. Grotjahn, G. Bertrand, R. Jazzar and K. M. Engle, *ACS Catal.*, 2022, **12**, 7243–7247.
44 S. Yazdani, G. P. Junor, J. L. Peltier, M. Gembicky, R. Jazzar, D. B. Grotjahn and G. Bertrand, *ACS Catal.*, 2020, **10**, 5190–5201.
45 S. K. Thakur, M. Kaur, K. K. Manar, M. Adhikari, A. R. Choudhury and S. Singh, *Chem. – Eur. J.*, 2022, **28**, e202202237.
46 S. Pelties and R. Wolf, *Z. Anorg. Allg. Chem.*, 2013, **639**, 2581–2585.
47 (*a*) N. M. Rajendran, N. Gautam, P. Sarkar, J. Ahmed, A. Das, S. Das, S. K. Pati and S. K. Mandal, *Chem. Commun.*, 2021, **57**, 5282–5285; (*b*) A. P. Singh, P. P. Samuel, H. W. Roesky, M. C. Schwarzer, G. Frenking, N. S. Sidhu and B. Dittrich, *J. Am. Chem. Soc.*, 2013, **135**, 7324–7329.
48 M. Nagyházi, Á. Lukács, G. Turczel, J. Hancsók, J. Valyon, A. Bényei, S. Kéki and R. Tuba, *Angew. Chem., Int. Ed.*, 2022, **61**, e202204413.
49 J. Deme, M. Nagyházi, Z. May, J. Hancsók, J. Valyon, S. Kéki, R. Tuba and G. Turczel, *React. Kinet., Mech. Catal.*, 2022, **135**, 2519–2531.
50 S. Chakrabortty, M. Kaur, M. Adhikari, K. K. Manar and S. Singh, *Inorg. Chem.*, 2021, **60**, 6209–6217.
51 H. Lebel, M. K. Janes, A. B. Charette and S. P. Nolan, *J. Am. Chem. Soc.*, 2004, **126**, 5046–5047.
52 C. Metallinos, F. B. Barrett, J. L. Chaytor and M. E. A. Heska, *Org. Lett.*, 2004, **6**, 3641–3644.
53 M. Nagyházi, B. Almási, Á. Lukács, A. Bényei, T. Nagy, S. Kéki and R. Tuba, *J. Mol. Struct.*, 2022, **1256**, 132483.
54 M. Kaur, M. Adhikari, K. K. Manar, Y. Yogesh, D. Prakash and S. Singh, *Inorg. Chem.*, 2024, **63**, 1513–1523.
55 P. Bharadwaz, R. D. Dewhurst and A. K. Phukan, *Adv. Synth. Catal.*, 2018, **360**, 4543–4561.
56 R. Logdi, A. Bag and A. K. Tiwari, *J. Mol. Graphics Modell.*, 2019, **93**, 107437.
57 S. Dutta, S. De, S. Bose, E. Mahal and D. Koley, *Eur. J. Inorg. Chem.*, 2020, **2020**, 638–655.
58 K. K. Manar, V. K. Porwal, R. S. Kamte, M. Adhikari, S. K. Thakur, D. Bawari, A. R. Choudhury and S. Singh, *Dalton Trans.*, 2019, **48**, 17472–17478.
59 N. Kuhn, G. Henkel, T. Kratz, J. Kreutzberg, R. Boese and A. H. Maulitz, *Chem. Ber.*, 1993, **126**, 2041–2045.
60 T. Böttcher, S. Steinhauer, L. C. Lewis-Alleyne, B. Neumann, H.-G. Stammler, B. S. Bassil, G.-V. Röschenthaler and B. Hoge, *Chem. – Eur. J.*, 2015, **21**, 893–899.
61 J. Monot, L. Fensterbank, M. Malacria, E. Lacôte, S. J. Geib and D. P. Curran, *Beilstein J. Org. Chem.*, 2010, **6**, 709–712.
62 P. K. Hota, S. Maji, J. Ahmed, N. M. Rajendran and S. K. Mandal, *Chem. Commun.*, 2020, **56**, 575–578.
63 J. L. Peltier, E. Tomás-Mendivil, D. R. Tolentino, M. M. Hansmann, R. Jazzar and G. Bertrand, *J. Am. Chem. Soc.*, 2020, **142**, 18336–18340.
64 N. Gautam, R. Logdi, P. Sreejyothi, N. M. Rajendran, A. K. Tiwari and S. K. Mandal, *Chem. Commun.*, 2022, **58**, 3047–3050.
65 A. D. Bage, T. A. Hunt and S. P. Thomas, *Org. Lett.*, 2020, **22**, 4107–4112.
66 G. Kundu, R. Dixit, S. Tothadi, K. Vanka and S. S. Sen, *Dalton Trans.*, 2022, **51**, 14452–14457.
67 N. Gautam, R. Logdi, S. P. A. Roy, A. K. Tiwari and S. K. Mandal, *Chem. Sci.*, 2023, **14**, 5079–5086.
68 S. Bansal, A. Biswas, A. Kundu, M. Adhikari, S. Singh and D. Adhikari, *ACS Catal.*, 2024, **14**, 8087–8095.
69 (*a*) B. Das, R. Yadav, A. Sharma, T. Karmakar and S. Kundu, *Chem. Commun.*, 2023, **59**, 5285–5288; (*b*) Y. Kim, J. E. Byeon, G. Y. Jeong, S. S. Kim, H. Song and E. Lee, *J. Am. Chem. Soc.*, 2021, **143**, 8527–8532.
70 A. Das, S. Saha, S. Maji, P. Sarkar, A. Jose, M. M. Bhatt, A. Bhunia, A. Dutta, S. K. Pati and S. K. Mandal, *Chem. – Eur. J.*, 2024, **30**, e202303411.
71 (*a*) M. Adhikari, S. De, K. K. Manar, S. K. Thakur, R. S. Kamte, D. Koley and S. Singh, *Eur. J. Inorg. Chem.*, 2024, e202400129; (*b*) Y. Wang, B. Quillian, P. Wei, C. S. Wannere, Y. Xie, R. B. King, H. F. Schaefer, P. V. R. Schleyer and G. H. Robinson, *J. Am. Chem. Soc.*, 2007, **129**, 12412–12413.
72 S. K. Thakur, S. De, M. Adhikari, K. K. Manar, D. Koley and S. Singh, *Chem. – Asian J.*, 2024, e202400730.
73 A. Doddi, M. Peters and M. Tamm, *Chem. Rev.*, 2019, **119**, 6994–7112.
74 M. Tretiakov, Y. G. Shermolovich, A. P. Singh, P. P. Samuel, H. W. Roesky, B. Niepötter, A. Visscher and D. Stalke, *Dalton Trans.*, 2013, **42**, 12940–12946.
75 A. Liske, K. Verlinden, H. Buhl, K. Schaper and C. Ganter, *Organometallics*, 2013, **32**, 5269–5272.
76 M. Adhikari, S. K. Thakur and S. Singh, *Eur. J. Inorg. Chem.*, 2023, e202300379.
77 Y. Wang, Y. Xie, P. Wei, R. B. King, H. F. SchaeferIII, P. v R. Schleyer and G. H. Robinson, *J. Am. Chem. Soc.*, 2008, **130**, 14970–14971.
78 O. Back, G. Kuchenbeiser, B. Donnadieu and G. Bertrand, *Angew. Chem., Int. Ed.*, 2009, **48**, 5530–5533.
79 R. Yadav, B. Das, A. Singh, Anmol, A. Sharma, C. Majumder and S. Kundu, *Dalton Trans.*, 2023, **52**, 16680–16687.
80 L. L. Liu, D. A. Ruiz, F. Dahcheh and G. Bertrand, *Chem. Commun.*, 2015, **51**, 12732–12735.
81 Y. Wang, H. P. Hickox, Y. Xie, P. Wei, D. Cui, M. R. Walter, H. F. Schaefer III and G. H. Robinson, *Chem. Commun.*, 2016, **52**, 5746–5748.

82 L. Gu, Y. Zheng, E. Haldón, R. Goddard, E. Bill, W. Thiel and M. Alcarazo, *Angew. Chem., Int. Ed.*, 2017, **56**, 8790–8794.
83 Y. Livshits-Kritsman, B. Tumanskii, G. Ménard and R. Dobrovetsky, *Chem. Commun.*, 2020, **56**, 1341–1344.
84 R. Yadav, A. Sharma, B. Das, C. Majumder, A. Das, S. Sen and S. Kundu, *Chem. – Eur. J.*, 2024, e202401730.
85 S. Gaillard and J.-L. Renaud, *Dalton Trans.*, 2013, **42**, 7255.
86 B. E. Maryanoff and R. O. Hutchins, *J. Org. Chem.*, 1972, **37**, 3475–3480.
87 (*a*) D. Pichon, M. Soleilhavoup, J. Morvan, G. P. Junor, T. Vives, C. Crévisy, V. Lavallo, J.-M. Campagne, M. Mauduit, R. Jazzar and G. Bertrand, *Chem. Sci.*, 2019, **10**, 7807–7811; (*b*) J. Lorkowski, D. Bouetard, P. Yorkgitis, M. Gembicky, T. Roisnel, N. Vanthuyne, D. Munz, L. Favereau, G. Bertrand, M. Mauduit and R. Jazzar, *Angew. Chem.*, 2023, **135**, e202305404; (*c*) M. Deng, N. F. M. Mukthar, N. D. Schley and G. Ung, *Angew. Chem.*, 2020, **132**, 1244–1247; (*d*) A. M. T. Muthig, J. Wieland, C. Lenczyk, S. Koop, J. Tessarolo, G. H. Clever, B. Hupp and A. Steffen, *Chem. – Eur. J.*, 2023, **29**, e202300946.

